Inorg. Chem. **2003**, *42*, 1211–1224

Iron–Arylimide Clusters $[Fe_m(NAr)_nCl_4]^{2-}$ (m, n = 2, 2; 3, 4; 4, 4) from a Ferric Amide Precursor: Synthesis, Characterization, and Comparison to Fe–S Chemistry

Jeremiah S. Duncan, Tamim M. Nazif, Atul K. Verma, and Sonny C. Lee*

Department of Chemistry, Princeton University, Princeton, New Jersey 08544

Received June 27, 2002

Tetrahedral $FeCl[N(SiMe_3)_2]_2(THF)$ (**2**), prepared from $FeCl_3$ and 2 equiv of $Na[N(SiMe_3)_2]$ in THF, is a useful ferric starting material for the synthesis of weak-field iron–imide (Fe–NR) clusters. Protonolysis of **2** with aniline yields azobenzene and $[Fe_2(\mu\text{-}Cl)_3(THF)_6]_2[Fe_3(\mu\text{-}NPh)_4Cl_4]$ (**3**), a salt composed of two diferrous monocations and a trinuclear dianion with a formal 2 Fe(III)/1 Fe(IV) oxidation state. Treatment of **2** with LiCl, which gives the adduct $[FeCl_2\{N(SiMe_3)_2\}_2]^-$ (isolated as the $[Li(TMEDA)_2]^+$ salt), suppresses arylamine oxidation/iron reduction chemistry during protonolysis. Thus, under appropriate conditions, the reaction of 1:1 **2**/LiCl with arylamine provides a practical route to the following Fe–NR clusters: $[Li_2(THF)_7][Fe_3(\mu\text{-}NPh)_4Cl_4]$ (**5a**), which contains the same Fe–NR cluster found in **3**; $[Li(THF)_4]_2[Fe_3(\mu\text{-}N\text{-}p\text{-}Tol)_4Cl_4]$ (**5b**); $[Li(DME)_3]_2[Fe_2(\mu\text{-}NPh)_2Cl_4]$ (**6a**); $[Li_2(THF)_7][Fe_2(\mu\text{-}NMes)_2Cl_4]$ (**6c**). $[Li(DME)_3]_2[Fe_4(\mu_3\text{-}NPh)_4Cl_4]$ (**7**), a trace product in the synthesis of **5a** and **6a**, forms readily as the sole Fe–NR complex upon reduction of these lower nuclearity clusters. Products were characterized by X-ray crystallographic analysis, by electronic absorption, ^1H NMR, and Mössbauer spectroscopies, and by cyclic voltammetry. The structures of the Fe–NR complexes derive from tetrahedral iron centers, edge-fused by imide bridges into linear arrays (**5a**,**b**; **6a**,**c**) or the condensed heterocubane geometry (**7**), and are homologous to fundamental iron–sulfur (Fe–S) cluster motifs. The analogy to Fe–S chemistry also encompasses parallels between Fe-mediated redox transformations of nitrogen and sulfur ligands and reductive core conversions of linear dinuclear and trinuclear clusters to heterocubane species and is reinforced by other recent examples of iron– and cobalt–imide cluster chemistry. The correspondence of nitrogen and sulfur chemistry at iron is intriguing in the context of speculative Fe-mediated mechanisms for biological nitrogen fixation.

Introduction

The molecular description of biological nitrogen fixation continues as a longstanding problem in inorganic chemistry.[1] A unique weak-field $[Fe_7MoS_9]$ cluster, the FeMo-cofactor, is generally accepted as the site of dinitrogen reduction in the best-studied form of the nitrogenase enzymes, yet the means by which this cluster transforms substrate remains very much a mystery. One line of speculation[2,3] holds that dinitrogen reacts as a bridging ligand to multiple iron sites at the center of the cofactor, becoming, in effect, part of the cluster core during turnover. Experimental evidence[3] for this conjecture, however, is nonexistent.

We are exploring the chemistry of the Fe−N bond in weak-field environments to gain insight into the proposed enzymatic interactions of iron and nitrogen.[4] Toward this end, we have developed ferrous chemistry that accomplishes

* To whom correspondence should be addressed. E-mail: sclee@chemvax.princeton.edu.

(1) Some recent reviews: (a) Christiansen, J.; Dean, D. R.; Seefeldt, L. C. *Annu. Rev. Plant Physiol. Plant Mol. Biol.* **2001**, *52*, 269. (b) Rees, D. C.; Howard, J. B. *Curr. Opin. Chem. Biol.* **2000**, *4*, 559. (c) Smith, B. E. *Adv. Inorg. Chem.* **1999**, *47*, 159. (d) Howard, J. B.; Rees, D. C. *Chem. Rev.* **1996**, *96*, 2965. (e) Burgess, B. K.; Lowe, D. J. *Chem. Rev.* **1996**, *96*, 2983. (f) Eady, R. R. *Chem. Rev.* **1996**, *96*, 3013.

(2) Some competing mechanistic proposals: (a) Dance, I. *J. Biol. Inorg. Chem.* **1996**, *1*, 581. (b) Sellmann, D.; Sutter, J. *J. Biol. Inorg. Chem.* **1996**, *1*, 587. (c) Coucouvanis, D. *J. Biol. Inorg. Chem.* **1996**, *1*, 594. (d) Pickett, C. J. *J. Biol. Inorg. Chem.* **1996**, *1*, 601. (e) Leigh, G. J. *Eur. J. Biochem.* **1995**, *535*, 171.

(3) Fe-mediated mechanisms have been the subject of considerable computational study, as referenced and reviewed in Appendix 1 of the following: (a) Lovell, T.; Li, J.; Liu, T.; Case, D. A.; Noodleman, L. *J. Am. Chem. Soc.* **2001**, *123*, 12392. Also see: (b) Lovell, T.; Li, J.; Case, D. A.; Noodleman, L. *J. Am. Chem. Soc.* **2002**, *124*, 4546. (c) Zhong, S.-J.; Liu, C.-W. *Polyhedron* **1997**, *16*, 653. (d) Shestakov, A. F. *Russ. Chem. Bull.* **1996**, *45*, 1827. (e) Machado, F. B. C.; Davidson, E. R. *Theor. Chim. Acta* **1995**, *92*, 315. (f) Plass, W. *J. Mol. Struct.* **1994**, *315*, 53.

10.1021/ic025825j CCC: $25.00
Published on Web 01/23/2003

Scheme 1

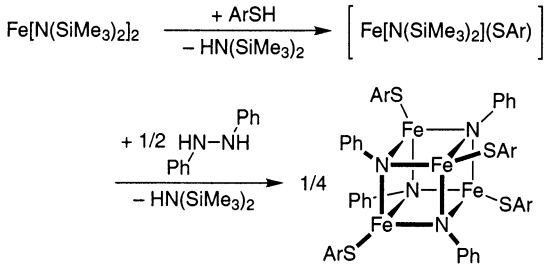

the 2-electron reduction of the N−N bond with concomitant assembly of a ferric imide cluster (Scheme 1), a synthetic transformation that might resemble the final stages of dinitrogen reduction.[5] The formation of iron−imide (Fe−NR) clusters in this system and the possibility of cluster-bound imides (or other anionic nitrogen fragments) as intermediates in the latter stages of nitrogenase action have prompted us to investigate the nature of Fe−NR clusters in general.

We describe here a new synthetic approach to the Fe−NR cluster manifold, with detailed characterization of the reaction chemistry and products. Our findings provide insight into the synthesis of Fe−NR clusters and reveal parallels between Fe−NR and iron−sulfur (Fe−S) chemistry that may have implications for the molecular description of biological nitrogen fixation.

Results and Discussion

Synthetic Considerations. The preparative chemistry of weak-field Fe−NR clusters is largely unexplored, comprising just three published studies, all recent.[4−7,8] In two accounts, clusters were assembled from reactions of iron halides and nitrogen anion (N-anion) reagents.[6,7] Although the use of these simple, accessible starting materials is synthetically attractive, we have found that the combination of exchange-labile, redox-active iron and aggressively reactive N-anions gives complex, difficult-to-control chemistry.[6]

An alternative, redox-linked synthesis of ferric arylimide clusters proceeds in good yield via bis(trimethylsilyl)amide complexes of Fe(II) (Scheme 1).[5] The $[N(SiMe_3)_2]^-$ ligand promotes chemical selectivity in this system in two ways. First, as a spectator ligand, its steric bulk enhances kinetic control at the high-spin metal center. Second, as a functional group, the coordinated amide serves as a powerful latent base[9] that can be replaced by other very basic ligands (e.g., imide) through protonolysis, thereby avoiding metathesis via N-anions. With these tactics in mind, we investigated direct routes to Fe−NR clusters using arylamines and sterically hindered amide complexes of Fe(III), as summarized in Scheme 2.

Scheme 2

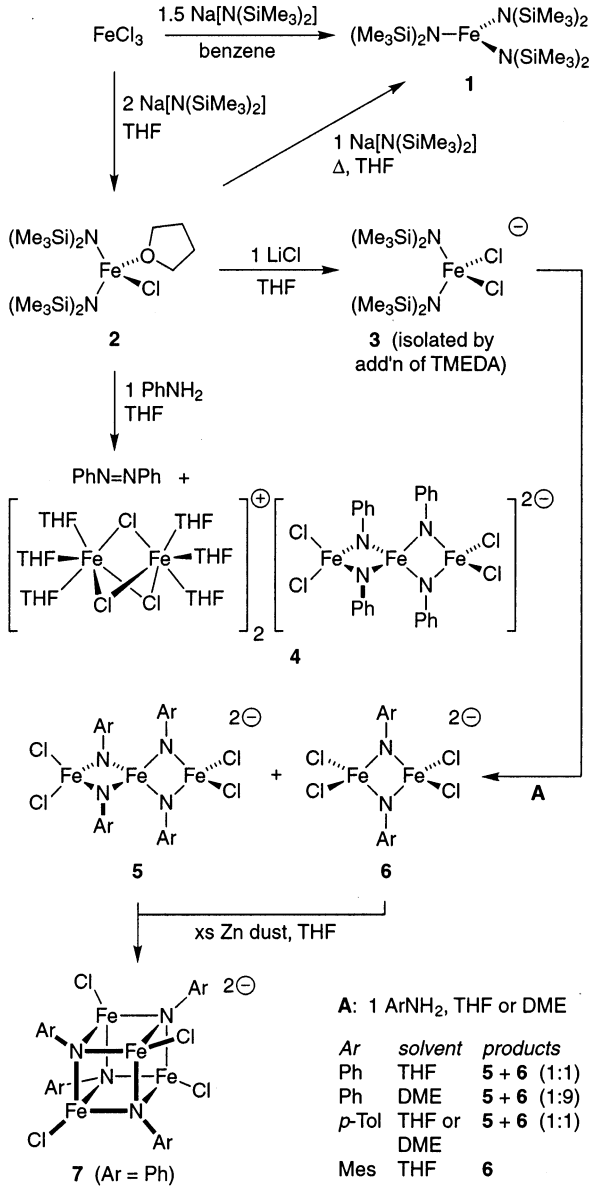

Ferric Amide Precursors. The ferric analogue of Fe-$[N(SiMe_3)_2]_2$ is trigonal planar $Fe[N(SiMe_3)_2]_3$ (**1**),[10] for which two different syntheses are known. The original preparation,[10a,c] conducted in arene solvents, works well despite the nonintuitive[11] 2:3 $FeCl_3$/$Na[N(SiMe_3)_2]$ stoichiometry. The other synthesis for tris(amide) **1**—the reaction

(4) Lee, S. C. Iron-Imide Clusters and Nitrogenase: Abiological Chemistry of Biological Relevance? In *Modern Coordination Chemistry: The Legacy of Joseph Chatt*; Leigh, G. J., Winterton, N., Eds.; Royal Society of Chemistry: Cambridge, U.K., 2002; pp 278−287.
(5) Verma, A. K.; Lee, S. C. *J. Am. Chem. Soc.* **1999**, *121*, 10838.
(6) Verma, A. K.; Nazif, T. M.; Achim, C.; Lee, S. C. *J. Am. Chem. Soc.* **2000**, *122*, 11013.
(7) Link, H.; Decker, A.; Fenske, D. *Z. Anorg. Allg. Chem.* **2000**, *626*, 1567.
(8) A limited number of iron clusters with phosphiniminate ($[R_3P{=}N]^-$) and sulfinimate ($[R_2S{=}N]^-$) core ligands are also known. Given that the properties of these monoanionic ligand types differ considerably from those of the dianionic imides of interest here, we exclude these clusters from further consideration: (a) Riese, U.; Harms, K.; Pebler, J.; Dehnicke, K. *Z. Anorg. Allg. Chem.* **1999**, *625*, 746. (b) Mai, H.-J.; Wocadlo, S.; Kang, H.-C.; Massa, W.; Dehnicke, K.; Maichle-Mössmer, C.; Strähle, J.; Fenske, D. *Z. Anorg. Allg. Chem.* **1995**, *621*, 705. (c) Roesky, H. W.; Seseke, U.; Noltemeyer, M.; Sheldrick, G. M. *Z. Naturforsch.* **1988**, *43b*, 1130. (d) Roesky, H. W.; Zimmer, M.; Schmidt, H. G.; Noltemeyer, M. *Z. Naturforsch.* **1988**, *43b*, 1490.
(9) (a) Comparative pK_a values in DMSO: MeOH, 29.0; *n*-BuSH, 17.0; $PhNH_2$, 30.6; PhOH, 18.0; PhSH, 10.3; Ph(H)NN(H)Ph, 26.2. Bordwell, F. G. *Acc. Chem. Res.* **1988**, *21*, 456. (b) In THF:^{i}Pr$_2$NH, 35.7. $(Me_3Si)_2NH$, 25.8. Fraser, R. R.; Mansour, T. S. *J. Org. Chem.* **1984**, *49*, 3443. Also see correction: *J. Org. Chem.* **1984**, *49*, 5284.

Table 1. Spectroscopic Data for Ferric Amide Complexes

complex	electronic abs:[a] λ, nm (ϵ_M, L·mol^{-1}·cm^{-1})	^{1}H NMR:[b] δ, ppm	
		$SiMe_3$	THF or TMEDA
$Fe[N(SiMe_3)_2]_3$ (**1**)[c]	345 (sh, 3500), 402 (5000), 498 (sh, 1500), 631 (1600)	33.5 (br)	
$FeCl[N(SiMe_3)_2]_2(THF)$ (**2**)	267 (6500), 433 (4500), 536 (sh, 1700)	15.5 (br)	43.0 (br), ca. 82 (v br)
$[Li(TMEDA)_2][FeCl_2\{N(SiMe_3)_2\}_2]$ (**3**)	269 (6900), 410 (3800), 474 (sh, 2500)	14.6 (br)	2.3 (br), 2.7 (br sh)

[a] *n*-Pentane (**1**) or THF (**2**, **3**) solution. [b] C_6D_6 solution, ca. 25 °C. [c] Our extinction coefficients are three times higher than literature values,[10d,e] due perhaps to sample decomposition in the original measurements; to our knowledge, ^{1}H NMR data have not been reported previously for **1**.

of 1:3 $FeCl_3$/Li[$N(SiMe_3)_2$] in THF—is not as straightforward as the literature implies.[10b] We have observed that, at room temperature, the reaction halts at a persistent deep red solution color which is obviously not the dark green of **1**; reflux is required to establish the expected color. Workup of the reaction at the intermediary red stage leads to the isolation of highly crystalline, dark-red $FeCl[N(SiMe_3)_2]_2$-(THF) (**2**).

Complex **2** is obtained directly in high yield (ca. 75%) by anion metathesis of $FeCl_3$ with exactly 2 equiv of Na-[$N(SiMe_3)_2$][12] in THF. The coordinated solvent is labile[13] and easily replaced by chloride; thus, dissolution of 1 equiv of LiCl in a deep red THF solution of bis(amide) **2** leads to a lighter, transparent red solution, from which, in the presence of TMEDA,[14] crystalline $[Li(TMEDA)_2][FeCl_2\{N(SiMe_3)_2\}_2]$ (**3**) can be isolated in quantity. Solution spectroscopic data for all three mononuclear ferric amide species (**1**−**3**) are presented for comparison in Table 1 and Figure 1. The color change upon LiCl addition is evident in the electronic absorption spectrum of **3**, which, in the visible range, is hypsochromic and slightly hypochromic relative to that of **2**. Both bis(amide) complexes are characterized by broad, paramagnetically shifted ^{1}H NMR signals, as expected for isolated high-spin ferric centers, with the methyl resonance of the anionic derivative located slightly upfield. The sterically derived kinetic stability of the heteroleptic, tetrahedral $[M\{N(SiMe_3)_2\}_2(L)(L')]^z$ environment is well-documented in early metals (groups 2−5 and f-elements), and Ti(III) and V(III) species exist that are isostructural to both

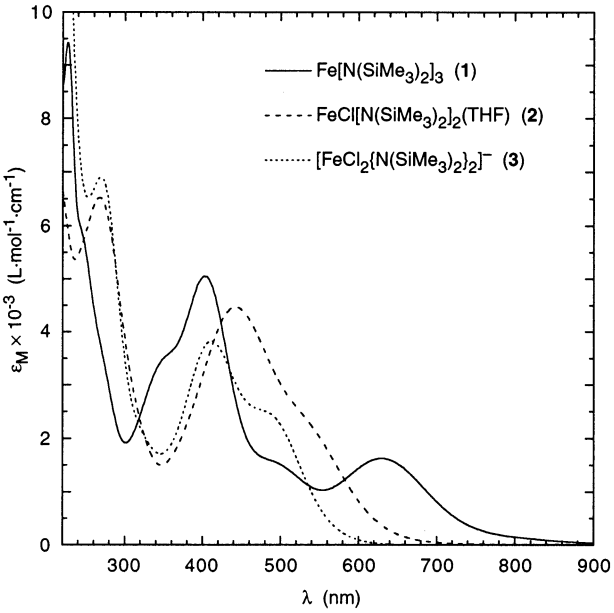

Figure 1. Comparative electronic absorption spectra of mononuclear ferric amide complexes in *n*-pentane (**1**) or THF (**2**, **3**).

2 and **3**;[15−18] aside from the present ferric complexes, however, we know of only four other examples of this ligand sphere involving transition elements (Cr(II) and Mn(II)) later than group 5.[19]

Crystallographic analyses of complexes **2** and **3** reveal related distorted tetrahedral iron sites (Table 2) that differ principally in the substitution of a THF ligand (Figure 2) by chloride (Figure 3). The steric demand of the amide ligands expands N−Fe−N and compresses Cl−Fe−O (**2**) or Cl−Fe−Cl (**3**) angles relative to the tetrahedral ideal, although replacement of the THF donor by the smaller, more distant chloride relieves some congestion, resulting in less pronounced angular distortions in **3**. The Fe−N contacts of **2** are similar to terminal iron−amide bond distances in tetrahedral environments[20] and in **1** (1.92 Å);[10h,i] Fe−N and

(10) Syntheses: (a) Bürger, H.; Wannagat, U. *Monatsh. Chem.* **94**, *1963*, 1007. (b) Alyea, E. C.; Bradley, D. C.; Copperthwaite, R. G. *J. Chem. Soc., Dalton Trans.* **1972**, 1580. (c) Bradley, D. C.; Copperthwaite, R. G. *Inorg. Synth.* **1978**, *18*, 112. Spectroscopic and magnetic properties: (d) Alyea, E. C.; Bradley, D. C.; Copperthwaite, R. G.; Sales, K. D.; Fitzsimmons, B. W.; Johnson, C. E. *Chem. Commun.* **1970**, 1715. (e) Alyea, E. C.; Bradley, D. C.; Copperthwaite, R. G.; Sales, K. D. *J. Chem. Soc., Dalton Trans.* **1973**, 185. (f) Bradley, D. C.; Copperthwaite, R. G.; Cotton, S. A.; Sales, K. D.; Gibson, J. F. *J. Chem. Soc., Dalton Trans.* **1973**, 191. (g) Fitzsimmons, B. W.; Johnson, C. E. *Chem. Phys. Lett.* **1974**, *24*, 422. Crystal structure: (h) Bradley, D. C.; Hursthouse, M. B.; Rodesiler, P. F. *Chem. Commun.* **1969**, 14. (i) Hursthouse, M. B.; Rodesiler, P. F. *J. Chem. Soc., Dalton Trans.* **1972**, 2100.

(11) Reaction at the limiting stoichiometry of 1:3 $FeCl_3$/Na[$N(SiMe_3)_2$] gives impurities that are difficult to separate from product.

(12) The use of the lithium salt is undesirable due to the formation of LiCl, which can contaminate the product even after pentane extraction and crystallization.

(13) Chemical exchange is evident upon doping of NMR solutions of **2** (C_6D_6) with THF: the resonances associated with bound THF disappear and are replaced by broadened signals at the diamagnetic shift positions of free THF. Despite the THF lability, **2** is recovered unchanged after multiple, successive recrystallizations from *n*-pentane.

(14) Adduct formation is reversible and crystallization attempts in the absence of TMEDA led to isolation of neutral **1**.

(15) $TiCl[N(SiMe_3)_2]_2(THF)$: Scoles, L.; Gambarotta, S. *Inorg. Chim. Acta* **1995**, *235*, 375.

(16) $[TiCl_2\{N(SiMe_3)_2\}_2]^-$: (a) Duchateau, R.; Gambarotta, S.; Beydoun, N.; Bensimon, C. *J. Am. Chem. Soc.* **1991**, *113*, 8986. (b) Beydoun, N.; Duchateau, R.; Gambarotta, S. *J. Chem. Soc., Chem. Commun.* **1992**, 244. (c) Putzer, M. A.; Magull, J.; Goesmann, H.; Neumuller, B.; Dehnicke, K. *Chem. Ber.* **1996**, *129*, 1401.

(17) $VCl[N(SiMe_3)_2]_2(THF)$: Berno, P.; Moore, M.; Minhas, R.; Gambarotta, S. *Can. J. Chem.* **1996**, *74*, 1930.

(18) $[VCl_2\{N(SiMe_3)_2\}_2]^-$: Gerlach, C. P.; Arnold, J. *Organometallics* **1997**, *16*, 5148.

(19) Cr(II) (planar): (a) Bradley, D. C.; Hursthouse, M. B.; Newing, C. W.; Welch, A. J. *J. Chem. Soc., Chem. Commun.* **1972**, 567. Mn(II): (b) Bradley, D. C.; Hursthouse, M. B.; Ibrahim, A. A.; Malik, K. M. A.; Motevalli, M.; Moseler, R.; Powell, H.; Runnacles, J. D.; Sullivan, A. C. *Polyhedron* **1990**, *9*, 2959. (c) Andruh, M.; Roesky, H. W.; Noltemeyer, M.; Schmidt, H.-G. *Z. Naturforsch., B* **1994**, *49*, 31.

Table 2. Selected Interatomic Distances (Å) and Angles (deg) in $FeCl[N(SiMe_3)_2]_2(THF)$ (**2**) and $[Li(TMEDA)_2][FeCl_2\{N(SiMe_3)_2\}_2]$ (**3**)[a]

	2 [X = O(1)]	**3** [X = Cl(2/4)]
Fe(1/2)−N(1/3)	1.902(2)	1.925(2)/1.918(2)
Fe(1/2)−N(2/4)	1.913(2)	1.930(2)/1.921(2)
Fe(1/2)−Cl(1/3)	2.2510(7)	2.279(1)/2.276(1)
Fe(1/2)−X	2.043(2)	2.269(1)/2.283(1)
N(1/3)−Fe(1/2)−N(2/4)	123.16(9)	120.2(1)/119.4(1)
N(1/3)−Fe(1/2)−Cl(1/3)	106.49(7)	103.90(9)/110.23(8)
N(2/4)−Fe(1/2)−Cl(1/3)	114.96(6)	111.38(8)/105.20(8)
N(1/3)−Fe(1/2)−X	112.54(8)	110.47(9)/103.65(8)
N(2/4)−Fe(1/2)−X	98.96(8)	105.15(9)/112.82(8)
Cl(1/3)−Fe(1/2)−X	97.61(5)	104.79(4)/104.69(4)
	Planarity	
N(1/3)[b]	0.157(2)	0.172(3)/0.157(3)
N(2/4)[b]	0.002(2)	0.020(3)/0.017(3)

[a] Divided entries refer to equivalent atoms and metrics of the two independent complexes in **3** in the order given, e.g., N(1/3)−Fe(1/2)−N(2/4) denotes two angles, N(1)−Fe(1)−N(2) and N(3)−Fe(2)−N(4); for the unique molecule in **2**, only the first atom number is used. [b] Perpendicular displacement from the [Fe, Si, Si′] plane.

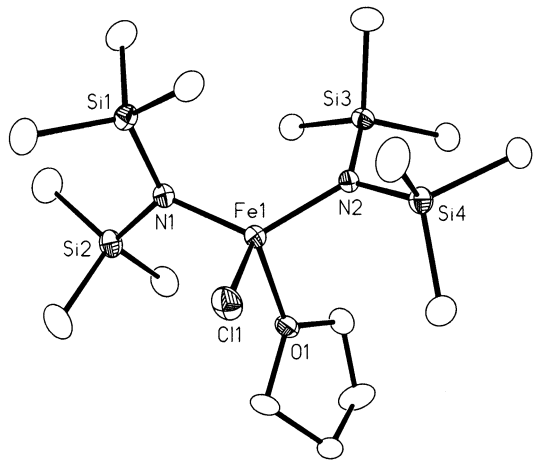

Figure 2. Structure of $FeCl[N(SiMe_3)_2]_2(THF)$ (**2**) with thermal ellipsoids (50% probability level) and selected atom labels. The THF ligand is partly disordered, and only one component is presented. For clarity in this and all subsequent structural depictions, carbon ellipsoids are presented without shading and hydrogen atoms are not shown.

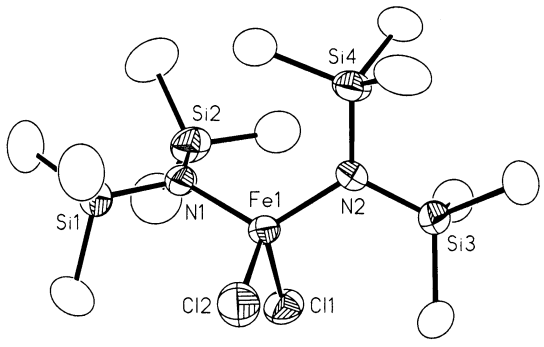

Figure 3. Anion structure of $[Li(TMEDA)_2][FeCl_2\{N(SiMe_3)_2\}_2]$ (**3**) with thermal ellipsoids (50% probability level) and selected atom labels. Only one of two independent complexes is presented.

Fe−Cl distances in anionic **3** are slightly longer, as expected from simple electrostatic considerations. In both complexes, the nitrogen atom of one amide is near planar, while the other amide nitrogen is somewhat pyramidalized. This distortion appears to correlate with eclipsing strain (or its avoidance) in the pyramidalized amide;[21] the $Me_3Si-N-SiMe_3$ wedge of this amide is almost coplanar with the THF oxygen (in **2**) or chloride (in **3**) when viewed along the Fe−N bond, while the planar amide adopts a perpendicular clinal conformation with respect to the same fiducial group.

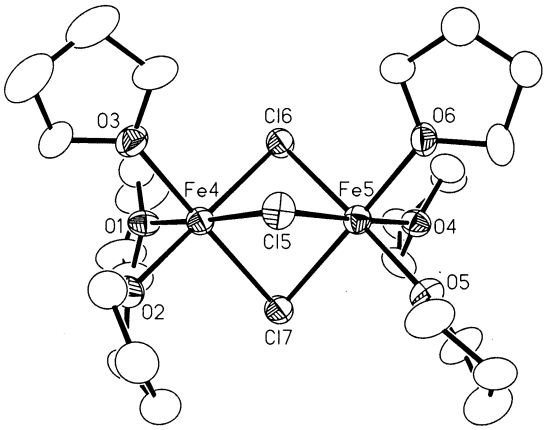

Figure 4. Cation structure of $[Fe_2(\mu\text{-}Cl)_3(THF)_6]_2[Fe_3(\mu\text{-}NPh)_4Cl_4]$ (**4**·THF) with thermal ellipsoids (35% probability level) and selected atom labels. Only one of two independent cations is presented. Selected distance ranges [mean] (Å) for the dimers: Fe−O, 2.105(5)−2.172(5) [2.14(2)]; Fe−Cl, 2.455(2)−2.513(2) [2.48(2)]; Fe···Fe, 3.051(2), 3.081(1) [3.07(2)].

In preliminary reactivity assays, tris(amide) **1** was found to be unsuitable as a protonolysis precursor, with test reactions returning the starting complex along with intractable, presumably polymeric material. This behavior suggests that the steric stability of **1** is such that the initial products of protonolysis, by virtue of reduced steric encumbrance, react further and much faster relative to remaining **1**. We therefore turned our attention to the less-hindered, bis(amide) complex **2**.

Protonolysis by Aniline. In principle, the protonolysis of **2** with 1 equiv of aniline provides a plausible stoichiometric route (eq 1) to a neutral Fe−NR heterocubane. In practice, a more complicated chemistry ensues. The addition of aniline to complex **2** in THF results in a rapid color change from deep red to black, with formation of insoluble dark precipitate. The THF-soluble components can be partitioned into an orange, pentane-soluble fraction consisting almost exclusively of azobenzene and a black, iron-containing solid that is insoluble in both *n*-pentane and benzene. Slow crystallization of this dark, THF-soluble material affords the cluster salt $[Fe_2(\mu\text{-}Cl)_3(THF)_6]_2[Fe_3(\mu\text{-}NPh)_4Cl_4]$ (**4**).

$$4FeCl[N(SiMe_3)_2]_2(THF)\ (\mathbf{2}) + 4PhNH_2 \rightarrow Fe_4(\mu_3\text{-}NPh)_4Cl_4 + 8(Me_3Si)_2NH + 4THF \quad (1)$$

Crystallographic structure analysis discloses two different cluster species in **4**. The first type consists of two octahedral iron centers, confacially bridged through three chloride ligands and terminally ligated by six THF donors (Figure 4). This structure has been observed elsewhere as a diferrous

(20) Stokes, S. L.; Davis, W. M.; Odom, A. L.; Cummins, C. C. *Organometallics* **1996**, *15*, 4521.

(21) The complexity of interactions and degrees of freedom within the $[M\{N(SiMe_3)_2\}_2(L)(L')]^z$ coordination sphere precludes any simple origin to the amide pyramidalization.

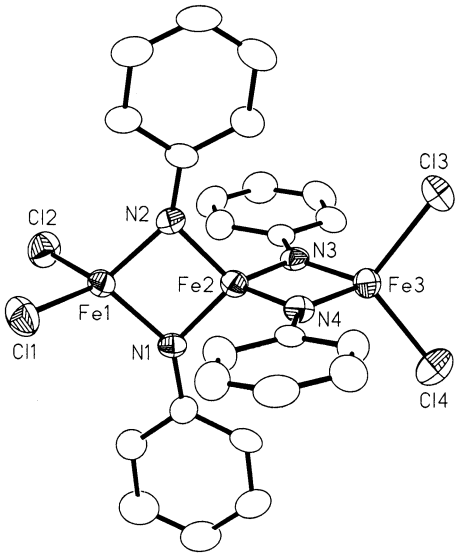

Figure 5. Anion structure of $[Fe_2(\mu\text{-}Cl)_3(THF)_6]_2[Fe_3(\mu\text{-}NPh)_4Cl_4]$ (**4**·THF) with thermal ellipsoids (35% probability level) and selected atom labels.

monocation.[22] The other cluster in compound **4** is a linear trinuclear array of tetrahedral iron centers with phenylimide bridges and terminal chloride ligands (Figure 5), details of which are presented later in comparison with other Fe−NR clusters. Two independent clusters of the dinuclear type and one trinuclear cluster occupy the asymmetric unit of the cell.

The assignment of cluster charge in **4** merits some consideration. The two $[Fe_2(\mu\text{-}Cl)_3(THF)_6]$ components are metrically indistiguishable from the known diferrous monocation,[22] suggesting the same +1 charge for each on structural grounds. If this is correct, the $[Fe_3(\mu\text{-}NPh)_4Cl_4]$ constituent must be a dianion with an unexpected 2 Fe(III)/1 Fe(IV) formal oxidation state. Conclusive evidence for this charge assignment comes from the isolation of $[Fe_3(\mu\text{-}NPh)_4Cl_4]^{2-}$ as an unambiguous dilithium salt (**6a**; vide infra) with an ^{1}H NMR signature identical to the predominant signal set found in crude **4**.

It is obvious that the reaction of the ferric amide precursor with aniline extends beyond simple protonolysis. Although the full mass balance for this reaction is unknown, the yield of azobenzene is sufficient to reduce ca. 22% of the starting Fe(III) to Fe(II); the formation of azobenzene as a significant coproduct thus implicates aniline, probably via ligated anilide or phenylimide, as the principal reductant in the system. By itself, the unexpected redox behavior need not preclude this synthesis as a viable route to Fe−NR chemistry. The redox-derived cation in **4**, however, is a source of chemically and spectroscopically active iron that hinders the study of the cluster of interest, and we therefore sought synthetic modifications to obtain more tractable product. Lithium chloride was effective for this purpose.

Practical Syntheses of Fe−NR Clusters. Treatment of a THF solution of 1:1 **2**/LiCl (which presumably contains $[FeCl_2\{N(SiMe_3)_2\}_2]^-$, based on the preparation of **3**)[23] with 1 equiv of aniline gives significantly altered chemistry relative to the original reaction without LiCl. Differences are immediately apparent: in the presence of LiCl, darkening of the reaction solution to opacity is slower (minutes vs seconds) and gives a different endpoint color (dark purple vs black), while the formation of insoluble solid and azobenzene is reduced to trace levels (<1% yield for azobenzene). Spectroscopic and crystallographic characterization of this modified reaction system (vide infra) reveals a product mixture consisting primarily of two Fe−NR components, dinuclear $[Fe_2(\mu\text{-}NPh)_2Cl_4]^{2-}$ and trinuclear $[Fe_3(\mu\text{-}NPh)_4Cl_4]^{2-}$, in roughly equimolar ratios; in addition, the tetranuclear heterocubane $[Fe_4(\mu_3\text{-}NPh)_4Cl_4]^{2-}$ forms as a minor byproduct (ca. 5 mol % relative to either the di- or trinuclear species). Only the triiron complex, the least soluble of the three clusters, has proven separable in quantity from this mixture as deep-brown, crystalline $[Li_2(THF)_7][Fe_3(\mu\text{-}NPh)_4Cl_4]$ (**5a**).

In DME solvent, the diiron phenylimide cluster forms as the predominant product (> 9:1 vs the triiron cluster), precipitating directly en masse as purple-black microcrystals of $[Li(DME)_3]_2[Fe_2(\mu\text{-}NPh)_2Cl_4]$ (**6a**). The immediate removal of poorly soluble **6a** from this reaction system may explain the limited formation of the trinuclear coproduct relative to the THF system. By contrast, the reaction of 1:1 **2**/LiCl with *p*-toluidine gives an approximate 1:1 mixture of the analogous di- and trinuclear clusters in either THF or DME solvent; here, the solubilizing effect of the *p*-Me group apparently allows sufficient solution concentrations to form the larger cluster in either solvent. The lower solubility of the triiron cluster again allows its bulk isolation by fractional crystallization as black $[Li(THF)_4]_2[Fe_3(\mu\text{-}N\text{-}p\text{-}Tol)_4Cl_4]$ (**5b**); the diiron coproduct, formulated as $Li_2[Fe_2(\mu\text{-}N\text{-}p\text{-}Tol)_2Cl_4]$ (**6b**), was identified in situ by NMR comparison with its phenylimide congener **6a**. The dinuclear Fe−NR core can also be stabilized through steric effects. Thus, protonolysis of 1:1 **2**/LiCl with mesidine in THF proceeds smoothly to give deep green solutions consisting exclusively of the diiron cluster, which can be crystallized in high yield as dark green $[Li_2(THF)_7][Fe_2(\mu\text{-}NMes)_2Cl_4]$ (**6c**). The absence of triiron product is attributed to destabilizing steric contacts that would exist between *o*-Me groups of adjacent mesitylimide ligands in the trinuclear geometry. Last, without LiCl, the reactions of *p*-toluidine or mesidine with **2** result in undefined iron-containing species and significant formation of the corresponding azoarenes.

Chemistry of Cluster Formation. The LiCl co-reagent supplies soluble, inert countercation (Li^+) and supplementary ligand (Cl^-) to the reaction system. While both components contribute to the synthesis and isolation of tractable Fe−NR species, the introduction of additional chloride appears central in regulating cluster assembly. As observed in **3**, available chloride is expected to cap metal coordination sites by replacing more labile solvent donors. The consequent stabilization of coordination spheres and inhibition of ligand exchange explain the slower rates for protonolysis, which presumably requires precoordination of incoming amine, as well as the near absence of insoluble, polymeric products. The inhibition of Fe(III)/arylamine redox chemistry (i.e.,

(22) Janas, Z.; Sobota, P.; Lis, T. *J. Chem. Soc., Dalton Trans.* **1991**, 2429.
(23) The direct use of **3** in cluster assembly was excluded in this study to avoid chemistry involving TMEDA and iron.

azoarene production) is also consistent with adduct formation, since the resulting anionic chloroferrate complexes should be less oxidizing than comparable neutral species. This is demonstrated in the cyclic voltammetry of **2** and **3**, which shows grossly irreversible reductions for both but with the peak potential of the anion shifted negative by 650 mV (0.1 M TBAP/MeCN, E_p^c vs SCE: **2**, −0.40 V; **3**, −1.05 V).

The use of LiCl does not eliminate metal-based redox chemistry altogether. Of the three cluster types isolated, only the diiron cluster represents a stoichiometrically exact protonolysis product (eq 2), yet it forms exclusively only with solubility or steric constraint. The triiron cluster, the coproduct under general conditions, is more oxidized than the starting materials, and its synthesis consequently entails intervening redox chemistry. We can offer a balanced, hypothetical reaction, using exact experimental reactant ratios, that couples the one-electron oxidation of the trinuclear cluster to the reduction of Fe(III) to Fe(II) (eq 3); the ligands are assumed to segregate as in cluster salt **4** such that imide donors ligate only to oxidized iron sites. Given the difficulties in tracking mass balance for this chemistry, it is not surprising that the minor[24] Fe(II) product predicted by eq 3 escapes detection, particularly if it occurs in the form of spectroscopically silent chloroferrous species.

$$2FeCl[N(SiMe_3)_2]_2(THF)\ (\mathbf{2}) + 2LiCl + 2ArNH_2 \rightarrow Li_2[Fe_2(\mu\text{-}NAr)_2Cl_4] + 4(Me_3Si)_2NH + 2THF \quad (2)$$

$$4FeCl[N(SiMe_3)_2]_2(THF)\ (\mathbf{2}) + 4LiCl + 4ArNH_2 \rightarrow Li_2[Fe_3(\mu\text{-}NAr)_4Cl_4] + Li_2[FeCl_4] + 8(Me_3Si)_2NH + 4THF \quad (3)$$

A small fraction of the Fe(II) is probably associated with the limited formation of the cubane dianion $[Fe_4(\mu_3\text{-}NPh)_4Cl_4]^{2-}$, which is reduced by two electrons relative to the neutral homologue expected from protonolysis alone (eq 1). Reducing conditions should therefore favor production of the cubane dianion, and indeed $[Li(THF)_4]_2[Fe_4(\mu_3\text{-}NPh)_4Cl_4]$ (**7**) is obtained as the sole soluble Fe−NR product when an exogenous reductant (Zn dust) is added to solutions of dinuclear **6a**, trinuclear **5a**, or crude 1:1 reaction mixtures of both.

We note finally that the dinuclear and cubane cluster dianions in **6a**,**c** and **7** have also been prepared, in different counterion form, from ill-defined reactions of iron chlorides and N-anion reagents.[7] These compounds were crystallographically characterized and possess Fe−NR cluster components that are metrically equivalent to the analogous structures described in the next section. Although synthetic analyses and solution characterizations were completely absent in the original account, we have ascertained, using spectroscopic data derived herein, that the underlying chemistry is quite complicated; the products reported do not, in fact, reflect the distribution of species actually generated by the reactions described.

(24) If the di- and trinuclear clusters are assumed as the sole products, forming in equimolar ratios according to eqs 2 and 3, one-sixth (17%) of the total iron content is predicted to be in the ferrous state.

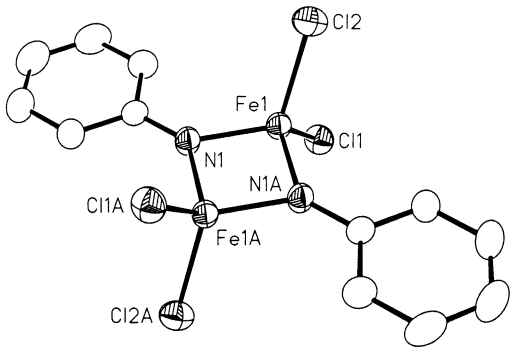

Figure 6. Anion structure of $[Li(DME)_3]_2[Fe_2(\mu\text{-}NPh)_2Cl_4]$ (**6a**) with thermal ellipsoids (50% probability level) and selected atom labels. Atoms with labels ending in "A" are generated by a crystallographic inversion center.

Fe−NR Cluster Structures. The Fe−NR clusters in this investigation all derive from tetrahedral iron centers that are edge-fused either through μ_2-imide bridges to form linear di- and trinuclear arrays or through μ_3-imide bridges to give the condensed tetranuclear heterocubane geometry; terminal chloride donors complete the ligand sets. The cluster types can be viewed in terms of a shared $[Fe_2N_2]$ rhombic motif (where N is the imide nitrogen) that completely defines the cores of the dinuclear clusters and constitutes the trimeric and heterocubane cluster geometries through vertex and edge fusion, respectively. The $[Fe_2N_2]$ fragments are rigorously planar for the dinuclear clusters due to lattice symmetry and near-planar for the others. The rhombs also approach mutual coplanarity with unhindered aryl subsituents as well, which argues for some degree of extended conjugation between the aryl π-orbitals, the imide lone pairs, and the iron centers. On average, the $[Fe_2N_2]$ polygons are almost square and exhibit only small rhombic angular distortions, with the exception of the trinuclear clusters described below. Cubane **7** has somewhat expanded $[Fe_2N_2]$ subunits due to lengthened Fe−N bonds from μ_3-imide bridging.

The structures of the dinuclear phenylimide and mesitylimide clusters possess crystallographic inversion symmetry, with a unique half-dimer in the asymmetric unit of **6a** (Figure 6) and two independent half-dimers for **6c** (Figure 7). The three structures show comparable interatomic metrics (Table 3) and differ significantly only in the orientation of the imide aryl substituents, which are coplanar with the $[Fe_2N_2]$ rhombic core in the phenyl cases but perpendicular in the mesityl derivative due to the steric demand of the *o*-Me groups. For one of the half-dimers in **6c** (Figure 7), a partially solvated $[Li(THF)_3]^+$ countercation interacts with one chloride ligand, leading to a moderately elongated Fe−Cl bond; all other cluster dianions are accompanied by well-separated, fully solvated counterions in the lattice.

Tetranuclear **7** (Figure 8) is one of several heterocubane clusters known in Fe−NR chemistry. The $[Fe_4(\mu_3\text{-}NR)_4]^z$ cores occur in a range of oxidation states: in addition to the $z = 2+$ state in **7**,[7] the $z = 4+$ core has been reported with arylimide bridges and terminal thiolate donors[5] and the $z = 3+$, $4+$, and $5+$ states have been reported with *tert*-butylimide bridges and terminal chloride donors (a terminal imide donor is also present in the most oxidized example).[6,7] Cluster

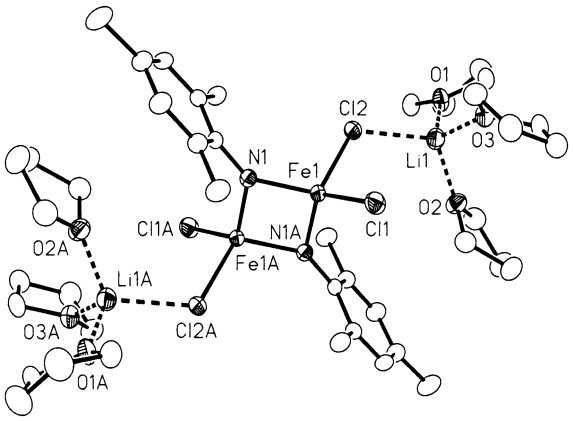

Figure 7. Structure of $[Li_2(THF)_7][Fe_2(\mu\text{-NMes})_2Cl_4]$ (**6c**) with thermal ellipsoids (50% probability level) and selected atom labels. Atoms with labels ending in "A" are generated by a crystallographic inversion center. One of two independent half-dimers is presented; the other dianion is well-separated from $[Li(THF)_4]^+$ cations and has no Li···Cl interactions.

Table 3. Selected Interatomic Distances (Å) and Angles (deg) in $[Li(DME)_3]_2[Fe_2(\mu\text{-NPh})_2Cl_4]$ (**6a**) and $[Li_2(THF)_7][[Fe_2(\mu\text{-NMes})_2Cl_4]$ (**6c**)[a]

	6a	**6c**
Fe(1/2)−N(1/2)	1.880(2)	1.867(2)/1.871(2)
Fe(1/2)−N(1A/2A)	1.881(2)	1.884(2)/1.879(2)
Fe(1/2)−Cl(1/3)	2.2703(8)	2.2619(6)/2.2901(6)
Fe(1/2)−Cl(2/4)	2.2647(8)	2.3191(5)/2.2838(6)
Fe(1/2)···Fe(1A/2A)	2.5517(7)	2.5188(5)/2.5506(5)
N(1/2)···N(1A/2A)	2.763(4)	2.779(3)/2.750(3)
N(1/2)−C^{ipso}	1.376(3)	1.389(2)/1.385(2)
N(1/2)−Fe(1/2)−N(1A/2A)	94.55(9)	95.63(7)/94.30(7)
Cl(1/3)−Fe(1/2)−Cl(2/4)	107.00(3)	106.01(5)/108.99(5)
N(1/2)−Fe(1/2)−Cl(1/3)	113.38(7)	117.99(5)/114.18(5)
N(1/2)−Fe(1/2)−Cl(2/4)	113.87(7)	110.16(5)/115.05(5)
N(1A/2A)−Fe(1/2)−Cl(1/3)	112.82(7)	115.76(5)/113.23(5)
N(1A/2A)−Fe(1/2)−Cl(2/4)	115.12(7)	112.26(5)/115.80(5)
Fe(1/2)−N(1/2)−Fe(1A/2A)	85.45(9)	84.37(7)/85.70(7)
Fe(1/2)−N(1/2)−C^{ipso}	137.0(2)	141.6(1)/138.3(1)
Fe(1A/2A)−N(1/2)−C^{ipso}	137.5(2)	134.0(1)/136.0(1)
Planarity and Torsion		
N(1/2)[b]	0.027(3)	0.022(2)/0.015(2)
N(1/2)−Ar[c]	5.15(3)	88.00(5)/89.24(4)

[a] Divided entries refer to equivalent atoms and metrics of the two independent half-dimers in **6c** in the order given, e.g., N(1/2)−Fe(1/2)−N(1A/2A) denotes two angles, N(1)−Fe(1)−N(1A) and N(2)−Fe(2)−N(2A); for the single half-dimer in **6a**, only the first atom number is used. [b] Perpendicular displacement from the [Fe, Fe′, C^{ipso}] plane. [c] Dihedral angle between the planar $[Fe_2N_2]$ rhomb and the least-squares-fitted aryl ring plane linked at the specified nitrogen.

core metrics generally expand upon reduction across the alkylimide series and upon subsitution of arylimide for alkylimide; cubane **7** follows these trends in possessing the longest Fe−N, Fe···Fe, and Fe−Cl contacts of all (Table 4).

The linear trinuclear core found in **4** and **5a**,**b** represents a new Fe−NR geometry. The structures of **4** (Figure 5) and **5b** (Figure 9) contain $[Fe_3(\mu\text{-NAr})_4Cl_4]^{2-}$ clusters with near identical core metrics (Table 5). In **5b**, the presence of two well-separated, $[Li(THF)_4]^+$ cations definitively establishes the dianionic charge of the trinuclear cluster, giving a formal oxidation state assignment of 2 Fe(III)/1 Fe(IV) to that complex and supporting the charges assigned previously for **4**. The μ_2-imide bridging is asymmetric, with Fe−N contacts about the central iron much shorter than those at the outer iron centers, which are comparable to equivalent bond lengths in the diferric dimers. The stabilization of the rare Fe(IV) state by N-anion ligands is well-documented;[6,25] the short Fe−N distances might therefore indicate localization of the

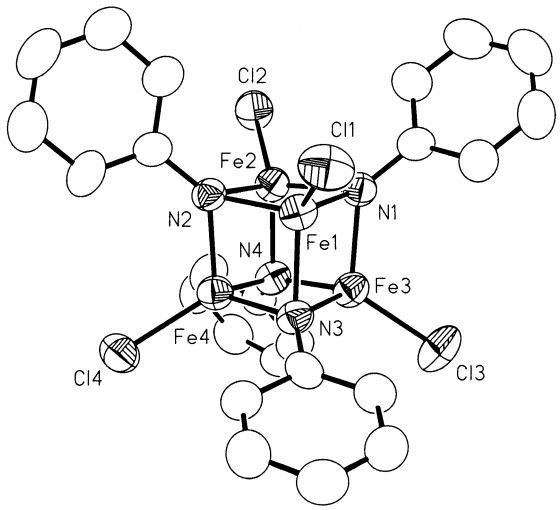

Figure 8. Anion structure of $[Li(DME)_3]_2[Fe_4(\mu_3\text{-NPh})_4Cl_4]$ (**7**·DME) with thermal ellipsoids (50% probability level) and selected atom labels.

Table 4. Selected Interatomic Distances (Å) and Angles (deg) in $[Li(DME)_3]_2[Fe_4(\mu_3\text{-NPh})_4Cl_4]$ (**7**·DME)[a]

Fe(1)−N(1/2/3)	1.974(4)/1.986(4)/1.986(4)
Fe(2)−N(1/2/4)	1.980(4)/1.984(4)/1.978(4)
Fe(3)−N(1/3/4)	2.000(4)/1.976(4)/1.988(4)
Fe(4)−N(2/3/4)	1.968(4)/1.994(4)/1.978(4)
Fe(1/2/3/4)−Cl(1/2/3/4)	2.217(2)/2.223(2)/2.228(2)/2.228(2)
N(1/2/3/4)−C^{ipso}	1.416(7)/1.404(6)/1.406(6)/1.404(7)
Fe(1)···Fe(2/3/4)	2.636(1)/2.608(1)/2.671(1)
Fe(2/2/3)···Fe(3/4/4)	2.689(1)/2.619(1)/2.681(1)
N(1)···N(2/3/4)	2.949(5)/2.988(6)/2.912(6)
N(2/2/3)···N(3/4/4)	2.918(6)/2.960(6)/2.916(6)
N(1/1/2)−Fe(1)−N(2/3/3)	96.3(2)/98.0(2)/94.6(2)
N(1/1/2)−Fe(2)−N(2/4/4)	96.1(2)/94.7(2)/96.7(2)
N(1/1/3)−Fe(3)−N(3/4/4)	97.5(2)/93.8(2)/94.7(2)
N(2/2/3)−Fe(4)−N(3/4/4)	94.9(2)/97.2(2)/94.5(2)
Cl(1)−Fe(1)−N(1/2/3)	119.5(1)/124.3(1)/118.3(1)
Cl(2)−Fe(2)−N(1/2/4)	122.8(1)/120.6(1)/119.6(1)
Cl(3)−Fe(3)−N(1/3/4)	120.9(1)/122.2(1)/121.1(1)
Cl(4)−Fe(4)−N(2/3/4)	119.3(1)/126.4(1)/118.1(1)
Fe(1/1/2)−N(1)−Fe(2/3/3)	83.6(2)/82.0(2)/85.0(2)
Fe(1/1/2)−N(2)−Fe(2/4/4)	83.2(2)/85.0(2)/83.0(2)
Fe(1/1/3)−N(3)−Fe(3/4/4)	82.3(2)/84.3(2)/85.0(2)
Fe(2/2/3)−N(4)−Fe(3/4/4)	85.4(2)/82.9(2)/85.1(2)
C^{ipso}−N(1)−Fe(1/2/3)	123.6(3)/131.7(3)/133.1(3)
C^{ipso}−N(2)−Fe(1/2/4)	129.1(3)/125.6(3)/133.7(3)
C^{ipso}−N(3)−Fe(1/3/4)	121.1(3)/133.4(3)/132.9(3)
C^{ipso}−N(4)−Fe(2/3/4)	126.0(3)/134.8(3)/125.9(3)
Fe(2/2/3)···Fe(1)···Fe(3/4/4)	61.68(3)/59.14(3)/61.03(3)
Fe(1/1/3)···Fe(2)···Fe(3/4/4)	58.65(3)/61.10(3)/60.67(3)
Fe(1/1/2)···Fe(3)···Fe(2/4/4)	59.67(3)/60.64(3)/58.38(3)
Fe(1/1/2)···Fe(4)···Fe(2/3/3)	59.77(3)/58.33(3)/60.95(3)

Planarity			
[Fe(1,2), N(1,2)][b]	0.057(2)	[Fe(2,3), N(1,4)][b]	0.069(1)
[Fe(1,3), N(1,3)][b]	0.026(2)	[Fe(2,4), N(2,4)][b]	0.026(2)
[Fe(1,4), N(2,3)][b]	0.072(1)	[Fe(3,4), N(3,4)][b]	0.057(2)

[a] Divided entries refer to separate, related atoms and their associated metrics in the order given, e.g., N(1/1/2)−Fe(1)−N(2/3/3) denotes three angles, N(1)−Fe(1)−N(2), N(1)−Fe(1)−N(3), and N(2)−Fe(1)−N(3). [b] Measured as the rms deviation from the least-squares-fitted $[Fe_2N_2]$ rhomb plane.

(25) Some examples: (a) Jüstel, T.; Müller, M.; Weyhermüller, T.; Kressl, C.; Bill, E.; Hildebrandt, P.; Lengen, M.; Grodzicki, M.; Trautwein, A. X.; Nuber, B.; Wieghardt, K. *Chem.—Eur. J.* **1999**, *5*, 793. (b) Cummins, C. C.; Schrock, R. R. *Inorg. Chem.* **1994**, *33*, 395. (c) Kostka, K. L.; Fox, B. G.; Hendrich, M. P.; Collins, T. J.; Rickard, C. E. F.; Wright, L. J.; Münck, E. *J. Am. Chem. Soc.* **1993**, *115*, 6746.

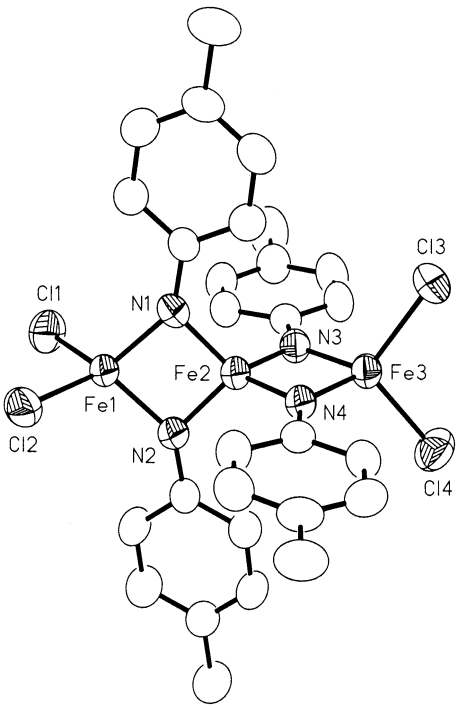

Figure 9. Anion structure of $[Li(THF)_4]_2[Fe_3(\mu_3\text{-N-}p\text{-Tol})_4Cl_4]$ (**5b**) with thermal ellipsoids (50% probability level) and selected atom labels.

high-valent ion to the central site, which has the most N-anion donors. For **5a**, the diffraction data were sufficient to resolve the trinuclear cluster and two solvated counterions, but extensive disorder precluded a detailed analysis.[26]

Spectroscopic Properties. Characteristic spectroscopic data for the Fe−NR clusters are summarized in Table 6. The electronic absorption spectra of the clusters in solution (Figure 10) are dominated by broad, intense charge-transfer bands at near-ultraviolet to blue energies that tail across the visible range. Molar absorptivities for the dinuclear clusters are approximately half those of the higher nuclearity clusters, and consequently, only the diiron clusters manifest distinguishable solution colors other than dark brown or black.

The Fe−NR clusters display well-defined, isotropically shifted ^{1}H NMR spectra that are consistent with ideal molecular symmetries and unrestricted N−Ar rotation (Figure 11). The resonances for the phenylimide ligands were assigned through integral ratios, which clearly identify the *p*-H signal, and paramagnetic relaxation effects, which associate the broadest peaks with the nuclei closest to the paramagnetic center (i.e., *o*-H protons); comparison with spectra of ring-substituted derivatives (i.e., **5b**, **6b**,**c**) further supports the assignments. All aryl-H resonances evince isotropic shifts[27] that alternate in sign with alternant hydrocarbon position (upfield for *o*- and *p*-H, downfield for *m*-H),

Table 5. Selected Interatomic Distances (Å) and Angles (deg) in the $[Fe_3(\mu\text{-NAr})_4Cl_4]^{2-}$ Clusters of $[Fe_2(\mu\text{-Cl})_3(THF)_6]_2[Fe_3(\mu\text{-NPh})_4Cl_4]\cdot$THF (**4**·THF) and $[Li(THF)_4]_2[[Fe_3(\mu\text{-N-}p\text{-Tol})_4Cl_4]$ (**5b**)[a]

	4·THF	**5b**
Fe(1)−N(1/2)	1.899(5)/1.892(6)	1.903(3)/1.896(3)
Fe(3)−N(3/4)	1.903(6)/1.903(6)	1.893(3)/1.886(3)
Fe(2)−N(1/2)	1.792(6)/1.797(5)	1.797(3)/1.799(3)
Fe(2)−N(3/4)	1.805(6)/1.793(6)	1.798(3)/1.805(3)
Fe(1)−Cl(1/2)	2.257(2)/2.262(2)	2.277(1)/2.266(1)
Fe(3)−Cl(3/4)	2.252(2)/2.247(2)	2.255(1)/2.246(1)
Fe(1/2)···Fe(2/3)	2.591(1)/2.582(1)	2.5963(7)/2.5814(7)
N(1/3)···N(2/4)	2.625(8)/2.652(9)	2.630(4)/2.637(5)
N(1/2)−C^{ipso}	1.389(8)/1.383(9)	1.391(5)/1.392(5)
N(3/4)−C^{ipso}	1.360(9)/1.379(9)	1.386(5)/1.384(5)
N(1/3)−Fe(1/3)−N(2/4)	87.7(2)/88.3(2)	87.6(1)/88.5(1)
Cl(1/3)−Fe(1/3)−Cl(2/4)	108.40(9)/106.75(9)	106.01(5)/108.99(5)
N(1)−Fe(1)−Cl(1/2)	117.1(2)/113.7(2)	115.1(1)/116.1(1)
N(2)Fe(1)-Cl(1/2)	113.3(2)/115.8(2)	116.9(1)/114.9(1)
N(3)−Fe(3)−Cl(3/4)	114.1(2)/116.2(2)	115.0(1)/115.0(1)
N(4)−Fe(3)−Cl(3/4)	115.1(2)/115.9(2)	112.4(1)/115.9(1)
N(1/3)−Fe(2)−N(2/4)	94.0(3)/94.9(3)	94.0(1)/94.1(2)
N(1)−Fe(2)−N(3/4)	117.1(3)/118.1(3)	116.2(1)/119.6(1)
N(2)−Fe(2)−N(3/4)	118.5(3)/116.1(3)	117.8(1)/117.2(1)
Fe(1)−N(1/2)−Fe(2)	89.1(2)/89.2(3)	89.1(1)/89.2(1)
Fe(2)−N(3/4)−Fe(3)	88.2(3)/88.6(3)	88.7(2)/88.7(2)
Fe(1)−N(1/2)−C^{ipso}	143.0(5)/142.9(5)	142.4(2)/143.1(3)
Fe(2)−N(1/2)−C^{ipso}	127.8(5)/127.5(5)	127.6(2)/131.3(3)
Fe(3)−N(3/4)−C^{ipso}	144.2(5)/142.8(5)	140.0(3)/138.8(2)
Fe(2)−N(3/4)−C^{ipso}	127.6(5)/128.6(5)	131.3(3)/132.4(3)
Fe(1)···Fe(2)···Fe(3)	179.56(6)	176.89(3)
	Planarity and Torsion	
N(1/2)[b]	0.04(1)/0.05(1)	0.027(4)/0.020(4)
N(3/4)[b]	0.003(6)/0.02(1)	0.007(3)/0.011(3)
[Fe(1,2), N(1,2)][c]	0.011	0.020
[Fe(2,3), N(3,4)][c]	0.001	0.014
Fe(1)N_2Fe(2)N_2Fe(3)[d]	88.6(2)	88.3(1)
N(1/2)−Ar[e]	10.7(2)/15.2(2)	15.15(8)/14.76(8)
N(3/4)−Ar[e]	1.9(3)/6.9(4)	2.5(2)/4.8(2)

[a] Divided entries refer to separate, related atom pairs and their associated metrics in the order given, e.g., N(1/3)−Fe(1/3)−N(2/4) denotes two angles, N(1)−Fe(1)−N(2) and N(3)−Fe(3)−N(4). [b] Perpendicular displacement from the [Fe, Fe′, C^{ipso}] plane. [c] Rms deviation from the least-squares-fitted $[Fe_2N_2]$ rhomb plane. [d] Dihedral angle between vertex-fused, least-squares-fitted $[Fe_2N_2]$ rhomb planes. [e] Dihedral angle between the least-squares-fitted $[Fe_2N_2]$ rhomb and aryl ring planes linked at the specified nitrogen.

reverse sign upon substitution of aryl-Me for aryl-H and do not attenuate with distance from the metal; these characteristics indicate that the shifts are propagated predominantly by a spin delocalization mechanism.[28] The magnitudes of the shifts fall into diagnostic ranges ($[Fe_3(\mu\text{-NAr})_4Cl_4]^{2-} \gg [Fe_2(\mu\text{-NAr})_2Cl_4]^{2-} > [Fe_4(\mu_3\text{-NAr})_4Cl_4]^{2-}$) that easily distinguish the cluster types in solution.

The electronic properties of the iron centers were investigated further using zero-field Mössbauer spectroscopy.[29] At 4.2 K, polycrystalline samples of dimeric **6a**,**c** each show a single, well-resolved quadrupole doublet with isomer shift

(26) Crystals of **5a** were obtained in two forms; both diffracted poorly and suffered from massive disorder of cation-associated solvent within a large asymmetric unit (two independent complexes). Parameters for crystals obtained by slow evaporation of THF at −30 °C: $[Li(THF)_4]_2[Fe_3(\mu\text{-NPh})_3Cl_4]$, space group $P2_1$ (No. 3), $Z = 4$, $a = 14.486(1)$ Å, $b = 18.495(1)$ Å, $c = 25.746(1)$ Å, $\beta = 90.437(4)°$, $V = 6897.3(8)$ Å^3, temperature = 200(2) K. For crystals obtained by THF/*n*-pentane diffusion at −30 °C: $[Li_2(THF)_7][Fe_3(\mu\text{-NPh})_3Cl_4]\cdot 3$THF, space group $P2_1/c$ (No. 14), $Z = 8$, $a = 21.882(2)$ Å, $b = 25.837(3)$ Å, $c = 24.657(3)$ Å, $\beta = 100.984(4)°$, $V = 13685(3)$ Å^3, temperature = 200(2) K.

(27) $(\Delta H/H_0)_{iso} = (\Delta H/H_0)_{dia} - (\Delta H/H_0)_{obs}$; $(\Delta H/H_0)_{dia}$ in CD_3CN, using arylamines as diamagnetic references (ppm): $PhNH_2$, 6.6 (*o*- and *p*-H), 7.08 (*m*-H); *p*-$TolNH_2$, 2.18 (Me), 6.54 (*o*-H), 6.90 (*m*-H); $MesNH_2$, 2.08 (*o*-Me), 2.14 (*p*-Me), 6.70 (*m*-H).

(28) (a) Horrocks, W. D., Jr. Analysis of Isotropic Shifts. In *NMR of Paramagnetic Molecules: Principles and Applications*; LaMar, G. N., Horrocks, W. D., Jr., Holm, R. H., Eds.; Academic Press: New York, 1973; Chapter 4. (b) Holm, R. H.; Phillips, W. D.; Averill, B. A.; Mayerle, J. J.; Herskovitz, T. *J. Am. Chem. Soc.* **1974**, *96*, 2109.

(29) (a) Münck, E. Aspects of ^{57}Fe Mössbauer Spectroscopy. In *Physical Methods in Bioinorganic Chemistry*; Que, L., Ed.; University Science Books: Sausalito, CA, 2000; pp 287−319. (b) Gütlich, P.; Link, R.; Trautwein, A. *Mössbauer Spectroscopy and Transition Metal Chemistry*; Springer-Verlag: Berlin, 1978.

Table 6. Spectroscopic Data for Fe−NR Clusters

cluster	electronic abs:[a] λ, nm (ϵ_M, L·mol^{-1}·cm^{-1})	^{1}H NMR:[b] δ, ppm			Mössbauer:[c] mm/s	
		o-H/Me	*m*-H	*p*-H/Me	d	$\lvert\Delta E_Q\rvert$
$[Fe_3(\mu\text{-NPh})_4Cl_4]^{2-}$ (**5a**)	260 (48 000), 412 (18 000), 693 (sh, 4800)	ca. −105 (v br)	99 (br)	−104 (br)	0.51 (67%) −0.21 (33%)	1.70 0.84
$[Fe_3(\mu\text{-N-}p\text{-Tol})_4Cl_4]^{2-}$ (**5b**)	256 (40 000), 432 (18 000), 700 (sh, 4800)	ca. −109 (v br)	101 (br)	113 (br)	0.37 (67%) −0.20 (33%)	1.13 0.85
$[Fe_2(\mu\text{-NPh})_2Cl_4]^{2-}$ (**6a**)	268 (21 000), 298 (sh, 13 000), 399 (7300), 456 (7900), 524 (6700)	−20.7 (br)	22.9	−22.8	0.44	1.21
$[Fe_2(\mu\text{-NMes})_2Cl_4]^{2-}$ (**6c**)	242 (22 300), 272 (21 800), 325 (sh, 12 600), 400 (sh, 11 500), 420 (13 200)	13.9 (br)	22.5	16.7	0.51	1.38
$[Fe_4(\mu_3\text{-NPh})_4Cl_4]^{2-}$ (**7**)	243 (45 000), 275 (sh, 35 000), 309 (sh, 28 000), 660 (4000)	−6.4 (br)	17.4	−8.8	0.57	1.32

[a] THF solution. [b] CD_3CN solution, ca. 25 °C; cation/lattice-associated solvent signals were also evident: DME (**6a**, **7**), 3.30 (s, Me), 3.47 (s, CH_2); THF (**5a**,**b**, **6c**), 1.81 (m), 3.65 (m). [c] Data were collected at 4.2 K (**6a**,**c**, **7**) or 200 K (**5a**,**b**), with isomer shifts referenced to Fe metal at room temperature; errors in fit estimated at ±0.02 mm/s.

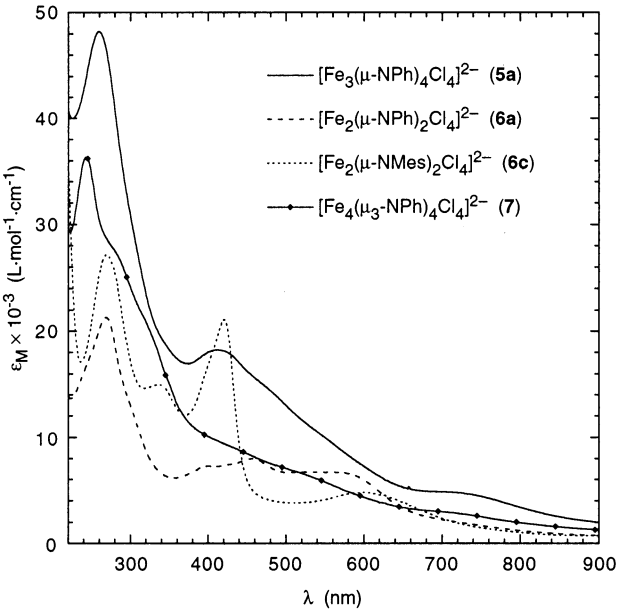

Figure 10. Comparative electronic absorption spectra of Fe−NR clusters in THF. The spectrum of **5b** is almost indisinguishable from that of **5a** and is not shown.

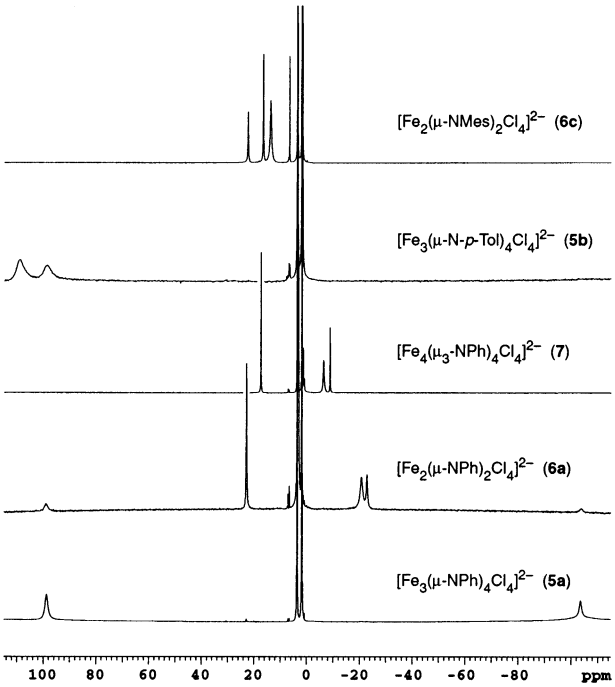

Figure 11. Comparative ^{1}H NMR spectra of Fe−NR clusters in CD_3CN. Signals in the diamagnetic region (δ 0−10 ppm) belong to residual protio solvent, cation/lattice-associated solvent (DME or THF), and arylamines arising from trace hydrolysis. Cluster **5a** is visible as a minor contaminant in the spectrum of **6a**.

and quadrupole splitting indicative of high-spin Fe(III). Under the same conditions, the mixed-valent cubane dianion **7** also presents a single symmetric quadrupole doublet of narrow line width, demonstrating that a single, valence-delocalized iron environment exists for this cluster on the spectroscopic time scale; the isomer shift is greater than those of the all-ferric dimers, as expected for a more reduced (mean: +2.5) iron oxidation state. The Mössbauer spectra of trinuclear **5a**,**b**, in contrast, exhibit broad magnetic features at 4.2 K that denote a paramagnetic ground state with intermediate spin relaxation;[30] these features collapse at 200 K to give spectra suggestive of two broad, overlapping quadrupole doublets. These latter spectra can each be simulated by a combination of two quadrupole doublets in a 2:1 ratio, with isomer shifts characteristic of valence-localized, high-spin Fe(III) and Fe(IV), respectively; this model must be treated with caution, however, as the doublets are not fully resolved at 200 K, but it is in accord with the oxidation state distribution suggested by cluster charge and structure.

(30) Yoo, S. J.; Angove, H. C.; Burgess, B. K.; Hendrich, M. P.; Münck, E. *J. Am. Chem. Soc.* **1999**, *121*, 2534.

Redox Behavior. The redox properties of the Fe−NR clusters were characterized by cyclic voltammetry in MeCN solution (Table 7). Measurements were conducted using 0.1 M (n-Bu_4N)Cl supporting electrolyte to suppress chloride ligand dissociation; the use of a more typical, noncoordinating electrolyte (0.1 M TBAP) led to ill-defined electrochemical responses. The following observations are noted:

(i) Redox processes for the di- and tetranuclear phenylimide clusters (**6a**, **7**) are irreversible. Voltammetric scans through the initial irreversible reduction of dinuclear **6a** lead to the development of secondary redox features associated with cubane **7**; this behavior echoes the reductive core conversion employed preparatively.

(ii) The diferric mesitylimide cluster **6c** is oxidatively more stable than its phenylimide counterpart (**6a**). The difference is significant, with **6c** displaying a reversible oxidation process along with an irreversible reduction that is shifted negative by 500 mV relative to the equivalent event in **6a**.

Table 7. Electrochemical Data[a] for Fe−NR and Analogous Fe−S Clusters

cluster	E_{ox}, V (ΔE_p, mV)	E_{red}, V (ΔE_p, mV)
$[Fe_3(\mu\text{-}Q)_4Cl_4]^{2-}$		
Q = NPh (**5a**)	+0.15 (80)	−0.85 (qrev[b])
Q = N-*p*-Tol (**5b**)	+0.04 (65)	−0.99 (qrev[b])
$[Fe_2(\mu\text{-}Q)_2Cl_4]^{2-}$		
Q = NPh (**6a**)	not obsd[c]	−1.48 (irrev)
Q = NMes (**6c**)	+0.15 (110)	<−1.7 (irrev)
Q = S[d]	not reported	−1.00 (irrev)
$[Fe_4(\mu_3\text{-}Q)_4Cl_4]^{2-}$		
Q = NPh (**7**)	−0.28 (irrev)	−1.57 (irrev)
Q = S[d]	not reported	−0.79 (90)

[a] $E^{ox/red}$ refer to the first oxidation/reduction potentials ($E_{1/2}$ for reversible and quasi-reversible couples, E_p^a or E_p^c for irreversible processes) measured at 100 mV/s scan rate and reported vs SCE; see Experimental Section for details. [b] Quasi-reversible behavior: for **5a**, ΔE_p = 140, 190, and 290 mV at 20, 100, and 500 mV/s scan rates, respectively, with $i_p^c/i_p^a \approx 1$ for all scans; for **5b**, ΔE_p = 310, 440, and 550 mV and $i_p^c/i_p^a \approx$ 1.3, 2.0, and 2.9 for 10, 100, and 250 mV/s scan rates, respectively. [c] The onset of chloride oxidation (from the supporting electrolyte) limits the upper scan range to ca. +0.20 V vs SCE. [d] From ref 34a.

(iii) The trinuclear arylimide clusters **5a**,**b** each exhibit a quasi-reversible reduction and a reversible oxidation. The reduction process is more reversible for the phenylimide trimer **5a** on the basis of peak current ratios and potential separations. The potential for this couple, which presumably represents the reduction of the trinuclear core to the all-ferric state, is much lower than the oxidation potential of $[FeCl_4]^{2-}$ (−0.04 V vs SCE, reversible);[31] these relative potentials therefore support the thermodynamic feasibility of the reaction outcome posited in eq 3, at least under the conditions of these voltammetric measurements.

(iv) The reversible oxidation events observed for **5a**,**b** and **6c** denote the existence of well-defined 2−/1− redox couples in these clusters. Although the nature of these oxidations, whether ligand- or metal-centered, is unknown at present, the reversibility of the couples and their modest oxidation potentials suggest that the oxidized species might be accessible for future study.

Fe−NR and Fe−S Chemistry: A Comparison. The Fe−NR chemistry developed in this study bears striking similarities to the well-established chemistry of Fe−S clusters. A structural commonality is immediately evident: if we assume congruency between imide and sulfide ligation, the three Fe−NR core geometries become isostructural with fundamental Fe−S cluster motifs[32] found in both biological[33] and synthetic systems. The pairing is exact for the di- and tetranuclear species, where equivalent Fe−NR and Fe−S clusters exist with identical terminal ligation and cluster charge.[34] For the trinuclear cores, the homology is less precise, as the Fe−S core is known only with thiolate terminal ligation and strictly in the all-ferric $[Fe_3(\mu\text{-}S)_4]^+$ state.[35] While the substitution of terminal thiolate ligands by chloride is well precedented in Fe−S cluster chemistry[34] and should be achievable in this instance, there is no evidence that the more oxidized $[Fe_3(\mu\text{-}S)_4]^{2+}$ core is sustainable with either thiolate or chloride ligation.

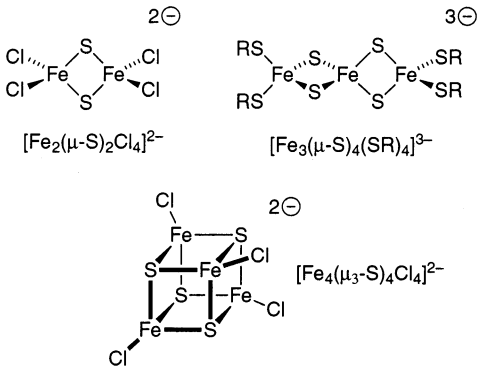

The relationship between Fe−NR and Fe−S reaction systems also includes characteristic aspects of chemical behavior. We have shown in this work and elsewhere that, under suitable Fe-NR synthesis conditions, weak-field iron species readily mediate both the 4-electron oxidative coupling of arylamine to azoarene and the 2-electron reduction of diarylhydrazines to iron-bound imide[5] (eqs 4 and 5). These interrelated redox transformations are equivalent in chemical context to sulfur-based half-reactions—the interconversions of organodisulfide/thiolate and elemental sulfur/polysulfide/sulfide (eqs 6 and 7)—ubiquitous in Fe−S chemistry.[32,35,36] In addition, the reductive transformations of the di- and trinuclear Fe−NPh clusters to cubane **7** fully replicate chemical and electrochemical core conversions of isostructural Fe−S complexes (eqs 8 and 9).[32a,34a,35]

$$Ar(H)N-N(H)Ar + 2e^- \rightleftharpoons 2[ArN]^{2-} + 2H^+ \quad (4)$$

$$2ArNH_2 \rightleftharpoons ArN{=}NAr + 4H^+ + 4e^- \quad (5)$$

$$RS-SR + 2e^- \rightleftharpoons 2RS^- \quad (6)$$

$$nS^0 + 2e^- \rightleftharpoons [S_n]^{2-} \rightleftharpoons S^{2-} \quad \text{(limit for } n = 1) \quad (7)$$

$$[Fe_2(\mu\text{-}S)_2Cl_4]^{2-} + 2e^- \rightarrow [Fe_4(\mu_3\text{-}S)_4Cl_4]^{2-} + 4Cl^- \quad (8)$$

$$[Fe_3(\mu\text{-}S)_4(SR)_4]^{3-} + FeCl_2 + RS^- \rightarrow [Fe_4(\mu_3\text{-}S)_4(SR)_4]^{2-} + 0.5RSSR + 2Cl^- \quad (9)$$

The occurrence of parallel nitrogen and sulfur chemistries is curious inasmuch as imide and sulfide ligands, while sharing the same formal charge, are not isoelectronic in a

(31) $[FeCl_4]^{2-}$ was generated in situ by addition of a small amount of $FeCl_2$ to a 0.1 M (*n*-Bu_4N)Cl/MeCN electrochemical solution.

(32) (a) Beinert, H.; Holm, R. H.; Münck, E. *Science* **1997**, *277*, 653. (b) Dance, I.; Fisher, K. *Prog. Inorg. Chem.* **1994**, *41*, 637 and references therein.

(33) The terminal cysteinate-ligated di-, tri-, and tetranuclear Fe−S cluster cores are biologically ubiquitous; the di- and tetranuclear clusters are native to a variety of metalloproteins in all organisms, and the trinuclear geometry has been observed as a stable, protein-bound isomer of a native biometallocluster under specific denaturing conditions.

(34) (a) Wong, G. B.; Bobrik, M. A.; Holm, R. H. *Inorg. Chem.* **1978**, *17*, 578. (b) Bobrik, M. A.; Hodgson, K. O.; Holm, R. H. *Inorg. Chem.* **1977**, *16*, 1851.

(35) (a) Hagen, K. S.; Watson, A. D.; Holm. R. H. *J. Am. Chem. Soc.* **1983**, *105*, 3905. (b) Hagen, K. S.; Holm, R. H. *J. Am. Chem. Soc.* **1982**, *104*, 5496.

(36) Representative preparative examples: Christou, G.; Garner, C. D. *J. Chem. Soc., Dalton Trans.* **1979**, 1093.

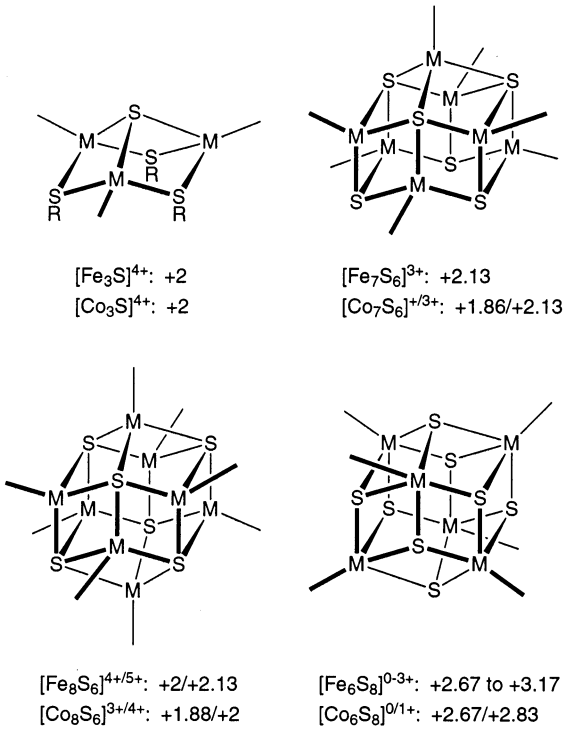

Figure 12. Homologous weak-field Fe−S and Co−S cluster cores with experimentally observed charges and mean oxidation states. The $[M_6(\mu_3\text{-}S)_8]$ geometry represents a strong-field environment[50] that is included here because of constitutional commonality (sulfide core, terminal phosphine ligation) with the other, weak-field examples.

strict sense[37] and differ considerably in essential properties that include basicity,[9] hard/soft character, bonding radii, and steric demand. One definite consequence of these dissimilarities is a marked stabilization of oxidized states in the imide clusters relative to their sulfide analogues. This is clearly evident in the first reduction potentials for analogous di- and tetranuclear Fe−NPh/Fe−S cluster pairs, which are shifted negative by 500−650 mV for the imide species (Table 7). Increased oxidative stability is further demonstrated by the trinuclear Fe−NR clusters, which are isolated in a state one electron more oxidized than their all-ferric Fe−S counterparts, and in the reversible electrochemical oxidations exhibited by these clusters and by the diferric cluster **6c**; the Fe−S clusters of interest here, by contrast, show no well-defined anodic processes whatsoever. Despite the differences, the qualitative chemical resemblance of nitrogen and sulfur at iron remain intriguing, especially in light of mechanistic proposals that invoke mixed Fe−S−N cluster cores as defining intermediates in the enzymatic reduction of dinitrogen.[2,3]

A recently reported cobalt−imide (Co−NR) cluster,[38] $[Co_8(\mu_3\text{-}NPh)_6(\mu\text{-}NPh)_3(PPh_3)_2]^-$, is pertinent to the present discussion. The octacobalt cluster is unmistakeable in its resemblance to the nitrogenase FeMo-cofactor. The structure of the latter derives primarily from macromolecular crystallography[39] and has yet to be attained in any synthetic Fe−S system. The Co−NR cluster nevertheless faithfully reproduces essential distinguishing features—the unsaturated trigonal metal centers, the open, nonrhombic cluster faces, and the singular core framework—of the cofactor geometry.[40]

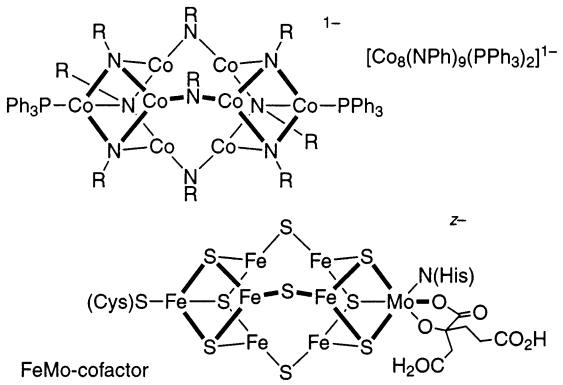

Under specific circumstances, weak-field Fe−S clusters are mirrored by cobalt−sulfur (Co−S) homologues with matching geometries, ligands, and charge states (Figure 12).[41−48] This homology depends not on electron counts but

(37) Basic symmetry considerations dictate that, in isolation, imide and sulfide have different degeneracies and relative orderings for their respective frontier orbitals; there is therefore no theoretical basis to expect a priori that the two ligand types will adopt the same bound structures. Isoelectronic arguments can only be made a posteriori once a shared ligation mode is evident and only for the complete metal−ligand unit.

(38) Link, H.; Fenske, D. *Z. Anorg. Allg. Chem.* **1999**, *625*, 1878.

(39) (a) Kim, J.; Rees, D. C. *Nature* **1992**, *360*, 553. (b) Chan, M. K.; Kim, J.; Rees, D. C. *Science* **1993**, *260*, 792. (c) Bolin, J. T.; Campobasso, N.; Muchmore, S. W.; Morgan, T. V.; Mortenson, L. E. In *Molybdenum Enzymes, Cofactors, and Model Systems*; Stiefel, E. I., Coucouvanis, D., Newton, W. E., Eds.; ACS Symposium Series 535; American Chemical Society: Washington, DC, 1993; pp 186−195. (d) Peters, J. W.; Stowell, M. H. B.; Soltis, S. M.; Finnegan, M. G.; Johnson, M. K.; Rees, D. C. *Biochemistry* **1997**, *36*, 1181. (e) Schindelin, N.; Kisker, C.; Sehlessman, J. L.; Howard, J. B.; Rees, D. C. *Nature* **1997**, *387*, 370. (f) Mayer, S. M.; Lawson, D. M.; Gormal, C. A.; Roe, S. M.; Smith, B. E. *J. Mol. Biol.* **1999**, *292*, 871.

(40) We believe the distinctive features of the cobalt cluster can be attributed partly to the steric influence of the imide substituents, much as trigonal planar iron is stabilized in **1** by its hindered amide ligands.

(41) $[Fe_3(\mu_3\text{-}S)]^{4+}$: Hagen, K. S.; Christou, G.; Holm, R. H. *Inorg. Chem.* **1983**, *22*, 309.

(42) $[Co_3(\mu_3\text{-}S)]^{4+}$: (a) Henkel, G.; Tremel, W.; Krebs, B. *Angew. Chem., Int. Ed. Engl.* **1983**, *22*, 318. (b) Also see ref 41.

(43) $[Fe_7(\mu\text{-}S)_3(\mu_3\text{-}S)_3]^{3+}$: Noda, I.; Snyder, B. S.; Holm, R. H. *Inorg. Chem.* **1986**, *25*, 3851.

(44) $[Co_7(\mu\text{-}S)_3(\mu_3\text{-}S)_3]^{+,3+}$: (a) Fenske, D.; Hachgenei, J.; Ohmer, J. *Angew. Chem., Int. Ed. Engl.* **1985**, *24*, 706. (b) Jiang, F.; Huang, L.; Lei, H.; Liu, H.; Kang, B.; Huang, Z.; Hong, M. *Polyhedron* **1992**, *11*, 361. (c) Jiang, F.; Lei, X.; Hong, M.; Huang, Z.; Kang, B.; Liu, H. *J. Organomet. Chem.* **1993**, *443*, 229.

(45) $[Fe_8(\mu_4\text{-}S)_6]^{4+,5+}$: (a) Pohl, S.; Saak, W. *Angew. Chem., Int. Ed. Engl.* **1984**, *23*, 904. (b) Pohl, S.; Opitz, U. *Angew. Chem., Int. Ed. Engl.* **1993**, *32*, 863. (c) Goh, C.; Segal, B. M.; Huang, J.; Long, J. R.; Holm, R. H. *J. Am. Chem. Soc.* **1996**, *118*, 11844.

(46) $[Co_8(\mu_4\text{-}S)_6]^{3+,4+}$: (a) Christou, G.; Hagen, K. S.; Holm, R. H. *J. Am. Chem. Soc.* **1982**, *104*, 1744. (b) Christou, G.; Hagen, K. S.; Bashkin, J. K.; Holm, R. H. *Inorg. Chem.* **1985**, *24*, 1010. (c) Hong, M.; Su, W.; Cao, R.; Jiang, F.; Liu, H.; Lu, J. *Inorg. Chim. Acta* **1998**, *274*, 229.

(47) $[Fe_6(\mu_3\text{-}S)_8]^{0-3+}$: (a) Cecconi, F.; Ghilardi, C. A.; Midollini, S. *J. Chem. Soc., Chem. Commun.* **1981**, 640. (b) Del Giallo, F.; Pieralli, F.; Fiesoli, L.; Spina, G. *Phys. Lett.* **1983**, *96A*, 141. (c) Agresti, A. Bacci, M.; Cecconi, F.; Ghilardi, C. A.; Midollini, S. *Inorg. Chem.* **1985**, *24*, 689. (d) Cecconi, F.; Ghilardi, C. A.; Midollini, S.; Orlandini, A.; Zanello, P. *J. Chem. Soc., Dalton Trans.* **1987**, 831. (e) Bencini, A.; Uytterhoeven, M. G.; Zanchini, C. *Int. J. Quantum Chem.* **1994**, *52*, 903. (f) Bencini, A.; Ghilardi, C. A.; Midollini, S.; Orlandini, A.; Russo, U.; Uytterhoeven, M. G.; Zanchini, C. *J. Chem. Soc., Dalton Trans.* **1995**, 963. (g) Goddard, C. A.; Long, J. R.; Holm, R. H. *Inorg. Chem.* **1996**, *35*, 4347.

on the mutual accessibility of shared oxidation states (this is characteristic of weak-field 3d environments, where metal−metal bonding and valence electron count have little value in rationalizing cluster structure compared to other, interrelated factors, such as oxidation state, ligand sphere, and net charge). As a practical matter, redox levels are dictated by cobalt,[49] a metal that strongly favors the divalent state under weak-field conditions,[50] even in the presence of imide donors.[38] The relation of Co−S to Fe−S and Fe−S to Fe−NR systems thus rationalizes the connection between the $[Co_8(NPh)_9]^-$ core and the $[Fe_7MoS_9]^z$ cofactor, which in turn strengthens the structural convergence of imide and sulfide ligation already noted on iron. The argument for oxidation state correspondence might also apply in the Co−NR analogue, where the average cobalt ion is +2.13, and the FeMo-cofactor, which is of uncertain charge; it is interesting that a mean iron level of +2.14 (1 Mo(IV)/6 Fe(II)/1 Fe(III)) has recently been proposed[51] for the resting form of cofactor.

Conclusions

The protonolysis of sterically hindered $FeCl[N(SiMe_3)_2]_2(THF)$ (**2**) by arylamines provides a new, serviceable route to Fe−NR cluster chemistry, allowing the isolation of $[Fe_2(\mu\text{-}NAr)_2Cl_4]^{2-}$, $[Fe_3(\mu\text{-}NAr)_4Cl_4]^{2-}$, and (with added reductant) $[Fe_4(\mu_3\text{-}NAr)_4Cl_4]^{2-}$ clusters in quantity under appropriate conditions. The protonolysis reactions are accompanied by Fe(III)-mediated redox events that oxidize arylamine to azoarene with formation of Fe(II) and probably disproportionate some of the iron to the +II and (formal) +IV states; the arylamine oxidation, which poses particular complications in cluster synthesis, can be controlled by the introduction of LiCl as a stoichiometric co-reagent.

The core frameworks of the Fe−NR clusters are constructed from tetrahedral iron centers and bridging imide ligation, organized into linear arrays for the di- and trinuclear examples or the more condensed heterocubane geometry in the tetranuclear case. The $[Fe_3(\mu\text{-}NAr)_4Cl_4]^{2-}$ cluster is notable for its unusual 2 Fe(III)/1 Fe(IV) formal oxidation state; structural and Mössbauer evidence suggest, but do not prove, a localized Fe(IV) assignment to the central iron site within the cluster. Distinctive isotropically shifted ^1H NMR spectra allow facile identification of the clusters in solution.

In a broader context, we find intriguing similarities of structure and reactivity linking Fe−NR and Fe−S chemistries. Weak-field Fe(II/III) complexes can mediate nitrogen redox chemistry at the N−N and N═N bond levels, fully reduced nitrogen incorporates readily as cluster-bound imide, and nitrogen chemistry at these iron centers resembles sulfur chemistry of Fe−S clusters. These observations reflect intrinsic properties of N-anions in a weak-field iron cluster environment and may therefore have bearing on chemical possibilities in iron-mediated mechanisms of nitrogenase action. The conspicuous parallels between abiological Fe−NR (and Co−NR) clusters and their Fe−S homologues provide a starting point for more detailed comparative investigation.

Addendum

The structure of the FeMo-cofactor has very recently been revised to include an interstitial light atom, believed to be nitride, within the center of the cluster core.[52] If correct, this discovery has significant ramifications for the molecular description of nitrogenase chemistry;[53] indeed, the presence of core-bound nitride may represent the first observational evidence for direct Fe participation in nitrogenase action. The existence of this unforeseen, biologically unprecedented ligand provides a compelling and timely argument for further exploration of iron/N-anion clusters as a tool to understand fundamental aspects of cofactor-relevant chemistry.

Experimental Section

Preparation of Compounds. All operations were performed under dry, anaerobic conditions (pure N_2 atmosphere) using standard protocols for the manipulation of air-sensitive compounds;[54] bench-top Schlenk operations were conducted in all-glass apparatus whenever possible. Except for anaerobic storage and handling, reagents were used as received (Acros, Aldrich, Cerac) unless otherwise noted. Solvents and liquid reagents were distilled from appropriate scavengers (ethers, *n*-pentane and benzene from sodium benzophenone ketyl, toluene from Na metal, amine reagents from CaH_2) and then degassed and kept over 4 Å molecular sieves; deuterated NMR solvents (Cambridge Isotope Laboratories) were dried by storage over 4 Å molecular sieves. Diatomaceous earth (Celite), LiCl, and alumina were dried/activated by heating at 150 °C (250−300 °C for alumina) for >12 h under dynamic vacuum.

Spectroscopic data for mononuclear ferric amide complexes and Fe−NR clusters are summarized in Tables 1 and 6, respectively.

(48) $[Co_6(\mu_3\text{-}S)_8]^{0,+}$: (a, b) Cecconi, F.; Ghilardi, C. A.; Midollini, S.; Orlandini, A. *Inorg. Chem. Acta* **1982**, *64*, L47; **1983**, *76*, L183. (c) Fenske, D.; Hachgenei, J.; Ohmer, J. *Angew. Chem., Int. Ed. Engl.* **1985**, *24*, 706. (d) Cecconi, F.; Ghilardi, C. A.; Midollini, S.; Orlandini, A.; Zanello, P. *Polyhedron* **1986**, *12*, 2021. (e, f) Hong, M.; Huang, Z.; Lei, X.; Wei, G.; Kang, B.; Liu, H. *Inorg. Chim. Acta* **1989**, *159*, 1; *Polyhedron* **1991**, *10*, 927. (g) Bencini, A.; Ghilardi, C.; Orlandini, A.; Midollini, S.; Zanchini, C. *J. Am. Chem. Soc.* **1992**, *114*, 9898. (h) Bencini, A.; Midollini, S.; Zanchini, C. *Inorg. Chem.* **1992**, *31*, 2132. (i) Jiang, F.-L.; Huang, Z.-Y.; Shi, J.-Q.; Lei, X.-J.; Hong, M.-C.; Lui, H.-Q. *Chin. J. Struct. Chem. (Jiegou Huaxue)* **1993**, *12*, 312. (j) Jiang, F.; Huang, X.; Cao, R.; Hong, M.; Liu, H. *Acta Crystallogr.* **1995**, *C51*, 1275. (k) Cecconi, F.; Ghilardi, C. A.; Midollini, S.; Orlandini, A.; Zanello, P.; Cinquantini, A,; Bencini, A.; Uytterhoeven, M. G.; Giorgi, G. *J. Chem. Soc., Dalton Trans.* **1995**, 3881.

(49) Cotton, F. A.; Wilkinson, G.; Murillo, C. A.; Bochmann, M. *Advanced Inorganic Chemistry*, 6th ed.; Wiley-Interscience: New York, 1999; pp 814−835.

(50) The exception to the divalent trend occurs for the $[M_6(\mu_3\text{-}S)_8]$ cores, which have oxidation levels closer to trivalent; the correlation between Fe/Co oxidation states persists nonetheless. Although the four cluster types in Figure 12 share the same basic σ- and π-donor ligands (core sulfides, terminal phosphines/halides/thiolates), the hexanuclear complexes possess 5-coordinate, square-pyramidal metal sites that are strong-field and low-spin (see refs 47f and 48 g,h); this explains the stability of the oxidized states. The other structure types contain 4-coordinate, weak-field metal sites.

(51) Lee, H. I.; Hales, B. J.; Hoffman, B. H. *J. Am. Chem. Soc.* **1997**, *119*, 11395.

(52) Einsle, O.; Tezcan, F. A.; Andrade, L. A.; Schmid, B.; Yoshida, M.; Howard, J. B.; Rees, D. C. *Science* **2002**, *297*, 1696.

(53) Lee, S. C.; Holm, R. H. Submitted for publication in *Proc. Natl. Acad. Sci. U.S.A.*

(54) (a) Shriver, D. F.; Drezdon, M. A. *The Manipulation of Air-Sensitive Compounds*, 2nd ed.; Wiley-Interscience: New York, 1986. (b) *Experimental Organometallic Chemistry*; Wayda, A. L., Darensbourg, M. Y., Eds.; ACS Symposium Series 357; American Chemical Society: Washington, DC, 1987.

Table 8. Crystallographic Data[a] for $FeCl[N(SiMe_3)_2]_2(THF)$ (**2**), $[Li(TMEDA)_2][FeCl_2\{N(SiMe_3)_2\}_2]$ (**3**), $[Fe_2(\mu\text{-}Cl)_3(THF)_6]_2[Fe_3(\mu\text{-}NPh)_4Cl_4]\cdot THF$ (**4**·THF), $[Li(THF)_4]_2[Fe_3(\mu\text{-}N\text{-}p\text{-}Tol)_4Cl_4]$ (**5b**), $[Li(DME)_3]_2[Fe_2(\mu\text{-}NPh)_2Cl_4]$ (**6a**), $[Li_2(THF)_7][Fe_2(\mu\text{-}NMes)_2Cl_4]$ (**6c**), and $[Li(DME)_3]_2[Fe_4(\mu_3\text{-}NPh)_4Cl_4]\cdot DME$ (**7**·DME)

	2	**3**	**4**·THF	**5b**	**6a**	**6c**	**7**·DME
formula	$C_{16}H_{44}N_2OFeClSi_4$	$C_{24}H_{68}N_6FeCl_2Si_4$	$C_{76}H_{124}N_4O_{13}Fe_7Cl_{10}$	$C_{60}H_{92}N_4O_8Fe_3Cl_4Li_2$	$C_{36}H_{70}N_2O_{12}Fe_2Cl_4Li_2$	$C_{46}H_{78}N_2O_7Fe_2Cl_4Li_2$	$C_{52}H_{90}N_4O_{14}Fe_4Cl_4Li_2$
fw	484.18	686.88	2047.23	1320.61	990.28	1038.48	1374.31
space group	$P\bar{1}$ (No. 2)	$P2_1/c$ (No. 14)	$P\bar{1}$ (No. 2)	$P2_1/n$ (No. 14)	$C2/c$ (No. 15)	$P2_1/c$ (No. 14)	$P2_1/n$ (No. 14)
Z	2	8	2	4	4	4	4
a, Å	8.3297(4)	19.2815(4)	13.4941(7)	14.4481(7)	29.231(1)	13.5238(4)	12.5052(6)
b, Å	11.4333(6)	22.4243(4)	14.7117(6)	32.386(2)	11.6925(5)	19.3851(6)	15.2469(8)
c, Å	15.7784(8)	19.5254(4)	23.627(1)	14.4685(8)	19.0941(8)	20.3408(7)	35.8276(19)
α, deg	105.188(2)		83.721(2)				
β, deg	92.640(2)	96.7900(8)	88.776(2)	91.610(2)	128.378(2)	94.911(1)	96.323(2)
γ, deg	109.323(2)		87.477(3)				
V, Å^3	1353.9(1)	8383.1(2)	4657.1(4)	6767.4(6)	5115.9(4)	5313.0(3)	6789.5(6)
ρ_{calcd}, g/cm^3	1.19	1.09	1.46	1.30	1.29	1.30	1.35
temp, K	140(2)	200(2)	200(2)	200(2)	200(2)	110(2)	200(2)
θ_{max}, deg	26.42	24.96	24.20	22.42	26.01	27.48	23.00
tot. data,[b] %	99.5	99.8	98.5	98.9	99.8	99.9	99.9
μ, mm^{-1}	0.841	0.623	1.403	0.844	0.827	0.794	1.014
R (wR2),[c] %	3.84 (9.01)	5.05 (12.25)	6.79 (13.38)	4.44 (10.97)	4.37 (10.78)	3.73 (8.00)	5.11 (14.86)
S[d]	1.065	1.030	1.029	1.034	1.015	1.022	1.014

[a] Data collected with graphite-monochromatized Mo Kα radiation ($\lambda = 0.71073$ Å) using ω scans. [b] Percent completeness of (unique) data collection within θ_{max} limit. [c] Calculated for $I > 2\sigma(I)$: $R = \Sigma||F_o| - |F_c||/\Sigma|F_o|$, $wR2 = \{\Sigma[w(F_o^2 - F_c^2)^2]/\Sigma[w(F_o^2)^2]\}^{1/2}$. [d] S = goodness of fit $= [\Sigma w(F_o^2 - F_c^2)^2/(n - p)]^{1/2}$, where n is the number of reflections and p is the number of parameters refined.

The products described herein may decompose over time, even in solid form under anaerobic conditions (e.g., **6c**); compounds were therefore stored at −30 °C to enhance stability. Sample instability/reactivity probably explains difficulties in obtaining satisfactory elemental analyses, which in some cases have given wildly inconsistent values for duplicate analyses of the same crystalline material; this problem has been noted previously for **1**.[10c,d]

$Fe[N(SiMe_3)_2]_3$ (1).[10] A modified literature synthesis[10a,c] was used. A solution of $Na[N(SiMe_3)_2]$ (2.220 g, 12 mmol) in benzene (50 mL) was slowly added to a stirred suspension of $FeCl_3$ (1.300 g, 8.0 mmol) in benzene (15 mL) at 4 °C (ice bath), producing an immediate dark green color. The mixture was allowed to warm to ambient temperature, stirred overnight, and then evaporated to dryness in vacuo. The residue was extracted with *n*-pentane (60 mL) and filtered; the filtrate was concentrated to ca. 5 mL and cooled to −20 °C to yield dark green, crystalline **1**, which was isolated and dried in vacuo (0.836 g). Concentration and cooling of the mother liquor gave a second crop (0.370 g). The isolated yield (total: 1.206 g, 56% based on amide) is limited primarily by high product solubility. The compound identity was confirmed by unit cell determination[10h,i] (170 K): trigonal, $a = 16.191(4)$ Å, $c = 8.422(8)$ Å, $V = 1912(5)$ Å^3.

$FeCl[N(SiMe_3)_2]_2(THF)$ (2). A cold (−2 °C NaCl/ice bath) solution of $Na[N(SiMe_3)_2]$ (24.86 g, 135 mmol) in THF (125 mL) was added to a stirred suspension of $FeCl_3$ (11.00 g, 67.8 mmol) in THF (200 mL) at −2 °C. The deep red reaction mixture was allowed to warm to ambient temperature, stirred overnight (>12 h), and then filtered through diatomaceous earth (Celite) to remove NaCl; the filter bed was washed with THF to recover trapped product. The filtrate and washings were combined, evaporated to dryness in vacuo with gentle heating, then dried further under dynamic vacuum (12 h) to remove entrained THF. The solid residue was subjected to several cycles of *n*-pentane extraction and filtration, after which the combined pentane extracts (ca. 850 mL) were volume reduced to 650 mL and cooled to −20 °C for 6 h. The resulting dark red, air-sensitive crystals were isolated by filtration and dried under dynamic vacuum (12 h) at 40 °C to give 13.73 g of **2**. The filtrate was volume reduced further to 100 mL and then 30 mL and cooled to obtain additional crops (7.89 and 2.54 g, respectively). Total yield: 24.16 g (73.6%). Anal. Calcd for $C_{16}H_{44}ClFeN_2OSi_4$: C, 39.69; H, 9.16; N, 5.79. Found: C, 39.63; H, 8.81; N, 6.50.

$[Li(TMEDA)_2][FeCl_2\{N(SiMe_3)_2\}_2]$ (3). A mixture of **2** (0.968 g, 2.0 mmol) and LiCl (0.085 g, 2.0 mmol) was stirred in THF (20 mL) for 12 h. The resulting transparent red solution was evaporated to give a viscous oil that was redissolved in *N*,*N*,*N*′,*N*′-tetramethylethylendiamine (TMEDA, 1.18 g, 10 mmol) and toluene (ca. 5 mL). This solution was maintained at ambient temperature for 2 d to give red microcrystals that were collected, washed with cold pentane (3 × 2 mL), and dried in vacuo to afford 1.08 g (78.6%) of **3**. Anal. Calcd for $C_{24}H_{68}Cl_2FeLiN_6Si_4$: C, 41.97; H, 9.98; N, 12.24. Found: C, 40.88; H, 9.92; N, 12.36.

$[Fe_2(\mu\text{-}Cl)_3(THF)_6]_2[Fe_3(\mu\text{-}NPh)_4Cl_4]$ (4). A solution of aniline (0.467 g, 5.0 mmol) in THF (10 mL) was added dropwise to a stirred solution of **2** (2.422 g, 5.0 mmol) in THF (90 mL). The resulting dark brown mixture was stirred for 19 h, filtered through diatomaceous earth (Celite), and washed with several portions of THF; a significant amount of THF-insoluble black precipitate was evident at this stage. The combined black filtrate (ca. 150 mL) was evaporated to dryness in vacuo and then extracted with *n*-pentane (100 mL) to give a dark orange filtrate and a black, pentane-insoluble powder. The filtrate was evaporated in vacuo to a dark orange glass that was identified as azobenzene (isolated yield: 55 mg, 0.30 mmol) by ^{1}H NMR and GC/MS analysis. The pentane-insoluble black powder was dissolved in THF (75 mL) and then filtered, and the black filtrate was concentrated to ca. 40 mL. Vapor diffusion of *n*-pentane into this solution at −30 °C over 2 weeks gave black microcrystalline **4**, which was filtered out, washed with *n*-pentane (ca. 10 mL), and dried under nitrogen flow. Yield: 0.275 g (18.5%, based on Fe and assuming **4**·THF crystal composition). We have been unable to recrystallize **4**; the compound was therefore characterized by crystallographic and NMR analysis.

$[Li_2(THF)_7][Fe_3(\mu\text{-}NPh)_4Cl_4]$ (5a). A mixture of **2** (0.968 g, 2.0 mmol) and LiCl (0.084 g, 2.0 mmol) was stirred in THF (20 mL) for 2 h. Neat aniline (0.183 mL, 0.187 g, 2.0 mmol) was then added, resulting in a solution color change solution (ca. 1−2 min) to purple-black. The reaction mixture was stirred for 12 h, evaporated to dryness, and extracted with *n*-pentane to remove azobenzene (spectrophotometrically quantitated at 0.87% yield based on aniline), giving 0.523 g of a glassy black powder. The solid material was treated with DME (50 mL) and filtered to give a dark brown filtrate and black precipitate. The precipitate was dissolved in THF (20 mL) and filtered; vapor diffusion of *n*-pentane into the filtrate at −30 °C over 4 d gave brown needles of **5a** that were isolated,

rinsed with THF (3 × 1 mL) followed by pentane (3 × 1 mL), and dried in vacuo for 2 h. Yield: 0.222 g (31.8%, based on analytical composition). Anal. Calcd for **5a**−2THF, $C_{44}H_{60}Cl_4Fe_3Li_2N_4O_5$: C, 50.42; H, 5.77; N, 5.34. Found: C, 50.50; H, 5.83; N, 4.94.

$[Li(THF)_4]_2[Fe_3(\mu\text{-}N\text{-}p\text{-}Tol)_4Cl_4]$ (5b). A mixture of **2** (0.968 g**,** 2.0 mmol) and LiCl (0.084 g, 2.0 mmol) was stirred in dimethoxyethane (DME, 20 mL) for 2 h. A DME solution (20 mL) of *p*-toluidine (*p*-$TolNH_2$, 0.107 g, 2.0 mmol) was then added, resulting in darkening of the solution (ca. 1−2 min) to black. The solution was stirred for 8 h and filtered to isolate a black precipitate (0.288 g). Dissolution of this precipitate in THF (10 mL), followed by vapor diffusion of *n*-pentane at −30 °C over 2 d, gave black, crystalline **5b** which was collected, rinsed with 1:1 THF/pentane (5 mL) followed by pentane (3 mL), and then dried in vacuo for 1.5 h. Yield: 0.182 g (25.6%, based on analytical composition). Anal. Calcd for **5b**−3.5THF, $C_{46}H_{64}Cl_4Fe_3Li_2N_4O_{4.5}$: C, 51.72; H, 6.04; N, 5.24. Found: C, 51.69; H, 5.55; N, 4.91.

$[Li(DME)_3]_2[Fe_2(\mu\text{-}NPh)_2Cl_4]$ (6a). A mixture of **2** (0.121 g, 0.25 mmol) and LiCl (0.011 g, 0.25 mmol) was stirred in DME (10 mL) for 2 h. Neat aniline (0.023 mL, 0.024 g 0.25 mmol) was then added, resulting in darkening (ca. 2 min) to a purple-black solution color. The mixture was stirred for 8 h and then filtered to collect the purple-black, microcrystalline precipitate, which was dried under N_2 flow for 5 min. The precipitate is >90% pure **6a** by NMR analysis and contaminated only by **5a**; the crystallization characteristics of **5a** and **6a** prevented further purification of this material. Yield: 0.109 g (88.1%).

$[Li_2(THF)_7][Fe_2(\mu\text{-}NMes)_2Cl_4]$ (6c). A mixture of **2** (1.46 g, 3.0 mmol) and LiCl (0.128 g, 3.0 mmol) was stirred in THF (20 mL) for 1 h. A THF solution (10 mL) of mesidine (2,4,6-trimethylaniline, $MesNH_2$, 0.408 g, 3.0 mmol) was then added slowly, resulting in a color change to dark-green. The solution was stirred for 12 h and then concentrated in vacuo to ca. 10 mL and diluted with 25 mL of pentane. After 4 h, the mixture was filtered to harvest the microcrystalline precipitate, which was washed with pentane (3 × 10 mL) and dried briefly in vacuo to afford dark green-gray **6c**. Yield: 1.107 g (71.1%). This compound decomposes both in solution and in the solid state over a period of days at ambient temperature; the solid product was therefore stored at −30 °C. Anal. Calcd for **6c**−5THF, $C_{26}H_{38}Cl_4Fe_2Li_2O_2N_2$: C, 46.06; H, 5.65; N, 4.13. Found: C, 46.24; H, 6.20; N, 3.73.

$[Li(DME)_3]_2[Fe_4(\mu_3\text{-}NPh)_4Cl_4]$ (7). A mixture of **2** (0.968 g, 2.0 mmol) and LiCl (0.085 g, 2.0 mmol) was stirred in THF (20 mL) for 4 h. Neat aniline (0.183 mL, 2.0 mmol) was then added, resulting in a darkening of the solution within 2 min (purple-black). The mixture was stirred for 6 h, after which Zn dust (0.066 g, 1.0 mmol) was added, giving a brown-black solution after an additional 12 h. Solvent removal in vacuo yielded a black glass, which was rinsed with 2:1 v/v DME/THF (80 mL) and filtered to remove a small amount of brown tar. The filtrate was allowed to stand at ambient temperature until small crystals formed (ca. 12 h) and then concentrated in vacuo to 60 mL and diluted with 20 mL of *n*-pentane. Storage at −30 °C for 2 d afforded black microcrystals of **7**, which were collected, rinsed with 1:1 v/v DME/*n*-pentane (5 mL) followed by *n*-pentane (5 mL), and dried in vacuo for 4 h. Yield: 0.350 g (69.0% based on analytical composition). Anal. Calcd for **7**−3DME, $C_{36}H_{50}Cl_4Fe_4Li_2N_4O_6$: C, 42.65; H, 4.97; N, 5.53. Found: C, 42.23; H, 5.01; N, 4.77.

X-ray Crystallography. Single crystals suitable for X-ray diffraction analysis were obtained from the following conditions and solvents: cooling to −30 °C of *n*-pentane (**2**, as dark red parallelopiped rods), THF (**6c**, as green needles), or DME (**7**·DME, as black blocks); THF/*n*-pentane vapor diffusion at −30 °C (**4**·THF, from the reaction system as black rods, and **5b**, as black needles); slow room-temperature evaporation of *n*-pentane (**3**, as translucent orange-red rods) or 1:3 DME/THF (**6a**, as purple flat needles).

General crystallographic procedures have been described elsewhere.[55] Essential crystallographic data for compounds in this work are summarized in Table 8. Crystals of **6c** decompose, perhaps from desolvation, after a few hours of beam exposure under a nitrogen stream at 200 K; data were therefore collected at 110 K. Disordered coordinated and/or lattice solvent molecules were found in the structures of **2**, **4**·THF, **5b**, **6a**,**c**, and **7**·DME; appropriate models and restraints were applied as needed. Specific details for individual structure determinations are available as Supporting Information.

Electrochemical Analyses. Cyclic voltammograms were recorded on an Analytical Instrument Systems DLK-60 electrochemical analyzer using platinum working and counter electrodes and a nonaqueous $Ag/AgNO_3$ (0.01 M) reference electrode. The MeCN solvent was distilled from CaH_2 and then dried further by storage over activated alumina, which was filtered off before use. For **2** and **3**, measurements were conducted using a standard three-electrode cell and 0.1 M (*n*-$Bu_4N)(ClO_4)$ (TBAP) supporting electrolyte in MeCN. For the Fe−NR clusters (**5a**,**b**, **6a**,**c**, **7**) and $[FeCl_4]^{2-}$, a dual compartment cell was used to separate the analyte solution (0.1 M (*n*-Bu_4N)Cl/MeCN), containing the working and counter electrodes, from the reference electrode (0.1 M TBAP/MeCN); a fine porosity frit connected the two compartments. Potentials were referenced internally to the ferrocene/ferrocenium ($Fc^{0/+}$) couple and then converted to the SCE scale ($Fc^{+/0} = +0.38$ V vs SCE in 0.1 M TBAP/MeCN).[56]

Other Physical Measurements. NMR spectra were acquired on Varian 300, 400, and 500 MHz spectrometers, with chemical shifts referenced to residual protiosolvent signals. Solution absorption spectra were recorded on a Hewlett-Packard 8453 diode array spectrophotometer; for the amide and imide complexes, concentrated solutions and 0.1 or 1 mm path length cells were necessary to minimize decomposition. Mössbauer spectra were collected on polycrystalline samples using a constant acceleration spectrometer.[57] GC/MS data were obtained on a Hewlett-Packard 5890 Series II gas chromatograph linked to a Hewlett-Packard 5971A mass selective detector. Elemental analyses were performed by the Microanalysis Laboratory at the School of Chemical Sciences, University of Illinois, Urbana, IL 61801, or by Oneida Research Services, Inc., Whitesboro, NY 13492.

Acknowledgment. We thank Dr. D. M. Ho (Princeton) for crystallographic guidance, Prof. C. Achim (Carnegie-Mellon) for helpful discussions and experimental assistance, and Prof. R. H. Holm (Harvard) for access to a Mössbauer spectrometer. The generous support of the Arnold and Mabel Beckman Foundation (Beckman Young Investigator Award) and the NSF (CAREER CHE-9984645) is gratefully acknowledged.

Supporting Information Available: Crystallographic data (CIF) and Mössbauer spectra (PDF). This material is available free of charge via the Internet at http://pubs.acs.org.

IC025825J

(55) Kayal, A.; Ducruet, A. F.; Lee, S. C. *Inorg. Chem.* **2000**, *39*, 3696.
(56) Connelly, N. G.; Geiger, W. E. *Chem. Rev.* **1996**, *96*, 877.
(57) Details of Mössbauer instrumentation and methods: Cen, W.; Lee, S. C.; Li, J.; MacDonnell, F. M.; Holm, R. H. *J. Am. Chem. Soc.* **1993**, *115*, 9515.